

4 - Petrology

INTRODUCTION

For the initial petrological characterisation of samples from CRP-3, we followed the practices adopted in previous CRP investigations (Cape Roberts Science Team, 1998, 1999). The primary division for investigations was based on grain size, corresponding to clasts (larger than 2 mm in diameter), sand grains and mudrocks. In addition to the down-core distribution of clasts, which were logged for clast type, number and dimensions, separate studies were also carried out on the different lithological clast types, which were subdivided into pre-Devonian basement clasts, sedimentary clasts (probably representing the Beacon Supergroup) and volcanic clasts (Ferrar Supergroup). As well as visual examination, each of the clast groups was described petrographically to better characterise the groups and to confirm macroscopic identifications. Unlike previous studies for the *Initial Reports*, uncovered, unstained thin sections were used to characterise the sand-grain fraction in sandstones. The modal counts, while still qualitative, are believed to be more accurate than those obtained previously using smear slides. Finally, XRD measurements, using an automated diffractometer system, were used to identify the types and distribution of clay minerals in sieved mudrock-fraction splits of fine-sediment samples; these were also separately analysed by XRD for their bulk mineralogy. Together, these methods were used mainly to document the provenance and downhole provenance variations in CRP-3.

DISTRIBUTION OF CLASTS

Petrological and distribution data collected on clasts from CRP-2/2A (Talarico et al., in press) indicated that their downcore modal and compositional variations provide a potential tool for unravelling the complex interplay between tectonic, volcanic and glaciomarine-sedimentary processes during the formation of the Victoria Land Basin and the uplift of the Transantarctic Mountains (TAM) in Cenozoic time. For instance, a pilot frequency analysis (in preparation) on clast population from CRP-2/2A (Sequences 9, 10, and 11) outlined periodicities possibly driven by Milankovitch orbital variations (100 Ka and 21 Ka). These preliminary results pointed to a previously undocumented but significant climatic influence on clast distribution. The CRP-3 clast dataset may potentially enlarge the application of this pilot study to a larger distribution-data population, thus providing further constraints on environmental interpretations.

An investigation of the distribution of clasts in CRP-3 was performed following the same procedure adopted in CRP-2/2A. We logged and counted 27 778 clasts on the basis of both lithology and grain size in the c. 823-m-thick Cenozoic section of CRP-3. This study also included sampling and thin-section examination of all lithologies to improve their characterisation (see sections below on Basement, Volcanic and Sedimentary Clasts for further detailed petrographical information).

The total number of clasts per unit length shows major variations from 0-10 counts *per* metre for mud- or sand-rich intervals (*e.g.* LSU 1.3) to >150 counts *per* metre for diamictite units (*e.g.* LSU 2.1) and conglomerate units (*e.g.* LSU 12.3). Sharp variations across lithological boundaries are commonly present, as well as within-unit fluctuations.

We distinguished five main lithological groups. Their main petrographical features and clast dimensions can be summarised as follows:

- 1) Dolerites s.l.. Generally medium-grained and fresh and common in all units. However, a few scattered occurrences of deeply altered granules and small pebbles were noted in LSU 3.1, 5.1, 6.1, 11.1, 12.4, 13.1 and at the bottom of LSU 15.2. Dolerite clasts show the widest range in size, ranging from granule to boulders as much as 2 m across;
- 2) Sedimentary rocks. These include at least 4 lithological types (see section on Sedimentary Clasts): quartz-arenites, poorly- to moderately-sorted sandstone, grey to black siltstones, and coal; these clasts mainly belong to the small-pebble class, apart from coal fragments, which mainly occur as granules;
- 3) Granitoids. These consist mainly of biotite±hornblende monzogranites, with minor occurrence of leucotonalite, mostly represented within the granule class (fragments of quartz and/or pink feldspar crystals, and lithic fragments);
- 4) Volcanic rocks and sub-volcanic rocks. This group includes very fine-grained dolerite, non-vesicular basalt and amygdale-bearing altered basalt. All of these varieties mainly form granules to small pebbles;
- 5) Metamorphic rocks. A variety of metamorphic rocks, ranging from basement rocks such as orthogneiss, paragneiss and marble, to low-grade metasedimentary rocks of various origins are represented in this class (see section on Basement Clasts). All of these rock types only occur as small pebbles.

The distribution of these different lithological types is schematically shown in figure 4.1. Both granitoids and dolerites are ubiquitous, with dolerite persistently forming the dominant lithology throughout the core. In contrast, all other lithologies show a more restricted distribution.

Volcanic and very fine-grained dolerite clasts are abundant and persistent in the upper 0-150 mbsf interval, but they form a sparse clast population below 150 mbsf, with dominant amygdale-bearing altered basalts. Further information on the distribution of different volcanic varieties is given in the section on Volcanic Clasts.

Sedimentary clasts show a wider distribution and are significantly more abundant below 150 mbsf. Coal fragments are very rare in the upper 150 m of the cored succession; only one occurrence was detected at 43 mbsf (LSU 1.2). In contrast, coal is persistently present from 159 mbsf downcore, and very abundant, particularly in LSU 7.1 and in the lower

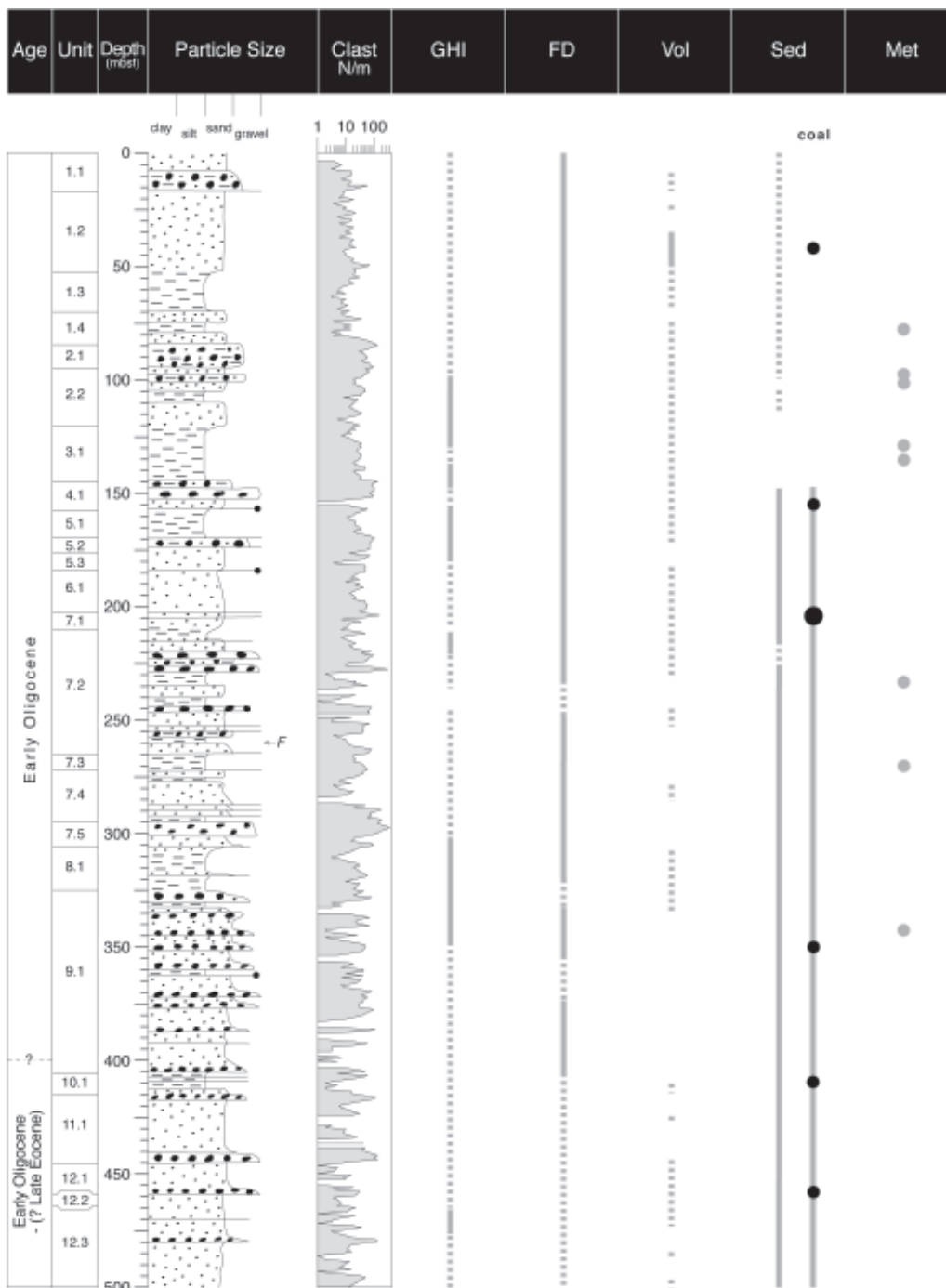


Fig. 4.1 - Distribution of main lithologies occurring as granule to boulder-grade clasts throughout CRP-3 core. Continuous lines indicate abundant (>15-20% total number of clasts) contents and persistent occurrence; dotted lines show intervals characterised by impersistent and/or very low occurrences. Small dots indicate the occurrence of few clasts (1-5); large dots, the occurrence of several clasts (>20). GHI: granitoids; FD: fine- to medium-grained dolerite; Vol: very fine-grained dolerite and non-vesicular basalts; Sed: sedimentary rocks; Met: metamorphic rocks. See text for further comments and discussion.

part of LSU 12.5.

Metamorphic rocks are definitely the least abundant of all represented lithologies and form scattered occurrences throughout the core (section on Basement Clasts and Fig. 4.2).

The analysis of distribution patterns of clasts allows preliminary provenance inferences and some constraints

on the uplift and erosional history of the Transantarctic Mountains. In agreement with conclusions drawn on provenance of clasts from drillcores CRP-1 (Talarico & Sandroni, 1998) and CRP-2/2A (Talarico et al., in press), preliminary petrographical data from CRP-3 confirm a local source, with the Cambro-Ordovician crystalline

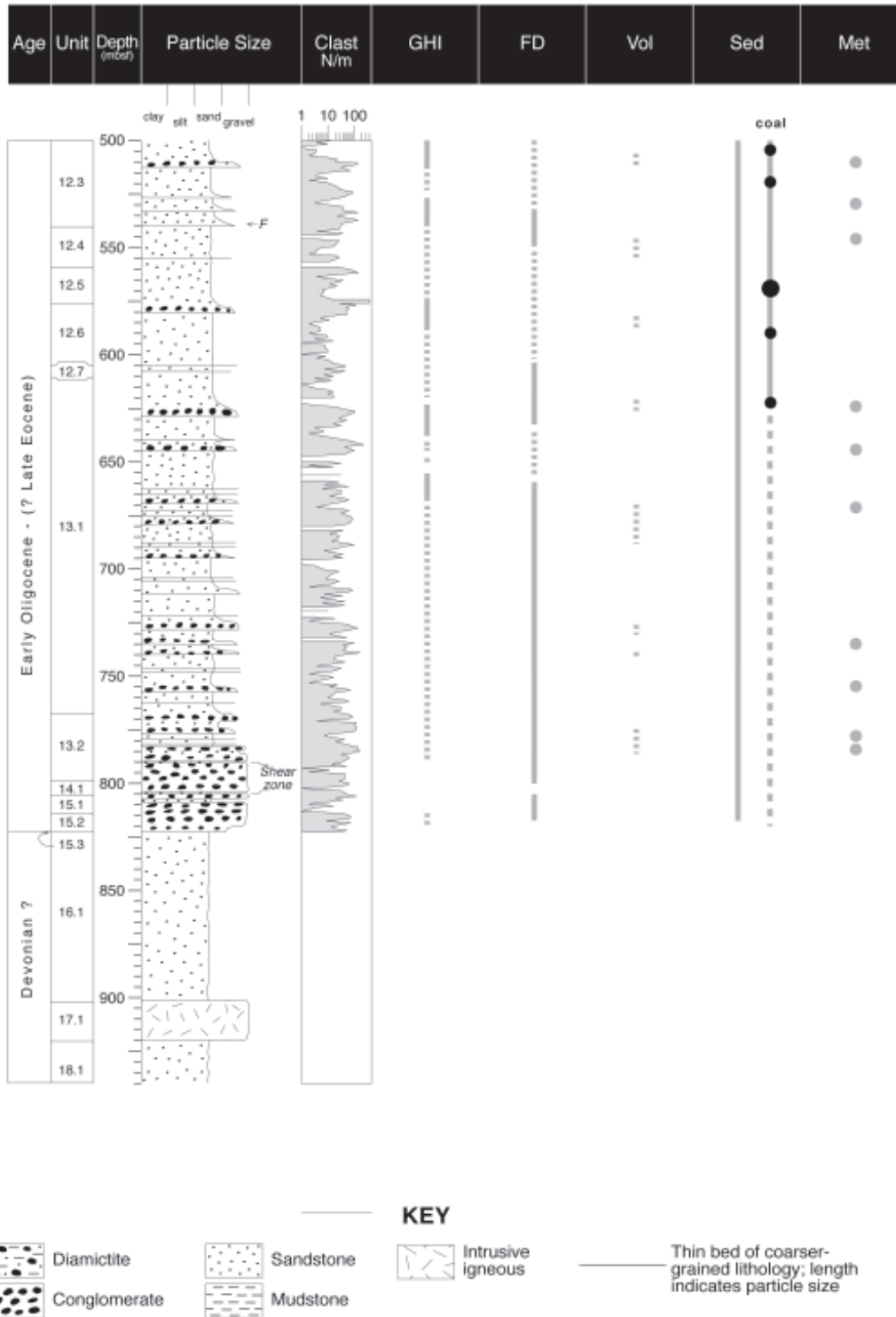


Fig. 4.1 - continued

basement, the Jurassic Ferrar Supergroup intrusive and volcanic suites, and the Devonian to Triassic Beacon Supergroup (Taylor and Victoria groups) acting as the major parent rock-units.

As demonstrated for CRP-2/2A (Talarico et al., in press), the compositional variability of clasts provides clear evidence of an evolving source area that documents stages of the erosional-tectonic evolution of the sector of the Transantarctic Mountains facing the CRP drilling sites. Unroofing of the deeper basement rocks should have occurred after an initial phase of erosion that primarily affected the uppermost part of the basement (near-Kukri peneplain zone) and the overlying cover rocks (the Taylor Group, the Ferrar Dolerite and, subordinately, the Kirkpatrick Basalt).

CRP-3 modal and compositional data indeed echo the same trends detected in the lowermost part of CRP-2/2A, providing another critical tie-boundary at *c.* 150 mbsf (which corresponds to seismic reflector, see section on Correlation of Seismic Reflectors). Similarly to the boundary located at 307 mbsf in CRP-2/2A, the *c.* 150 boundary in CRP-3 points to a relatively rapid provenance change from a lower clast assemblage sourced mainly from the Beacon Supergroup (including the Weller Coal Measures) and the Ferrar Supergroup (including the stratigraphically upper Kirkpatrick Basalt), to an upper clast assemblage mainly derived by Ferrar Supergroup rock units. It is noteworthy that the influx of detritus derived from granitic basement rock units, although impersistent and with variable, generally low proportions, was continuous throughout most of the depositional record, suggesting that the sub-Kukri basement was exposed even in the earliest part of the sedimentary history of western Victoria Land Basin at CRP-3.

BASEMENT CLASTS

As in previous drillholes (MSSTS-1, CIROS-1, CRP-1, CRP-2/2A) on the western edge of the Victoria Land Basin (Hambrey et al., 1989; Cape Roberts Science Team, 1998a, 1998d; Talarico & Sandroni, 1998; Talarico et al., in press), the CRP-3 borehole provides clear evidence of a multi-component source for the supply of granule- to boulder-sized clasts to the Cenozoic sedimentary sequences in the McMurdo Sound. This varied provenance closely mirrors the present-day on-shore geological units of the Transantarctic Mountains in southern Victoria Land, and among these units, those comprising granitoid and amphibolite-facies metasediments of the early Paleozoic Ross Orogen are a major component.

We focus on the preliminary petrographical examination of pre-Devonian basement clasts and clasts of metamorphosed sedimentary rocks within the lower Oligocene-?Late Eocene strata of the CRP-3 drillhole. It includes the description of all clasts belonging to the

granule, pebble and cobble grain-size classes, and some inferences concerning the most likely source-rock units. Sampling, macroscopic observations, and preliminary petrographical analyses (polarized-light microscopy) were performed following the same procedures and sample management adopted for CRP-1 and CRP-2/2A (Cape Roberts Science Team, 1998b, 1998c, 1999).

RESULTS

Clast counts in CRP-3 (see section on Distribution of Clasts) indicate that basement clasts are highly variable throughout the cored interval, but basement clasts are systematically less abundant than other lithologies (particularly dolerite and sedimentary rocks). In terms of dimension, finer pebbles (diameters <1 cm) and granules generally prevail over larger-sized clasts, which are very few and unevenly scattered (Fig. 4.2).

Granule-sized debris mainly consist of quartz and lesser feldspar, but pebble-sized clasts offer a significantly wider range of lithological types. The main lithological types can be grouped into two major groups: granitoids and less common metamorphic rocks.

Figure 4.2 shows the lithological range, distribution and position of the different rock types within the lithostratigraphical units identified in the CRP-3 core. Forty samples representative of all lithological types were collected and are listed in table 4.1. The table includes information on the lithology, the most relevant petrographical features (namely, textural, microstructural and alteration data), the most likely source-rock units in the crystalline basement of South Victoria Land, and stratigraphical position.

Granitoid pebbles consist of dominant grey, biotite-bearing monzogranite, pink biotite-hornblende monzogranite and biotite-bearing leucomonzogranite (Fig. 4.3). Minor lithologies include: actinolite-bearing leucotonalite, biotite-muscovite leucogranite, biotite porphyry, foliated biotite leucomonzogranite, and biotite-hornblende microdiorite. Preliminary microscopic examination revealed that all granitoid types show a variably developed low- to very-low-grade metamorphic alteration; allanite, zircon/monazite, apatite and rare tourmaline were found to be the most common accessory minerals in all granitoids.

The group of metamorphic clasts includes both rocks of igneous (namely granitic) derivation (mylonitic biotite with or without garnet orthogneiss, hornblende-bearing biotite orthogneiss) and metasedimentary rocks, including muscovite-tourmaline quartzite, biotite-bearing meta-quartz arenite, biotite±calcite meta-siltstone, biotite-clinoamphibole meta-marl, calcite-clinoamphibole-biotite-metafeldsarenite, graphite-bearing marble, sillimanite-biotite paragneiss, and calcite-biotite schist.

Microscopic examination of selected metamorphic clasts suggests that these rocks reflect a rather wide

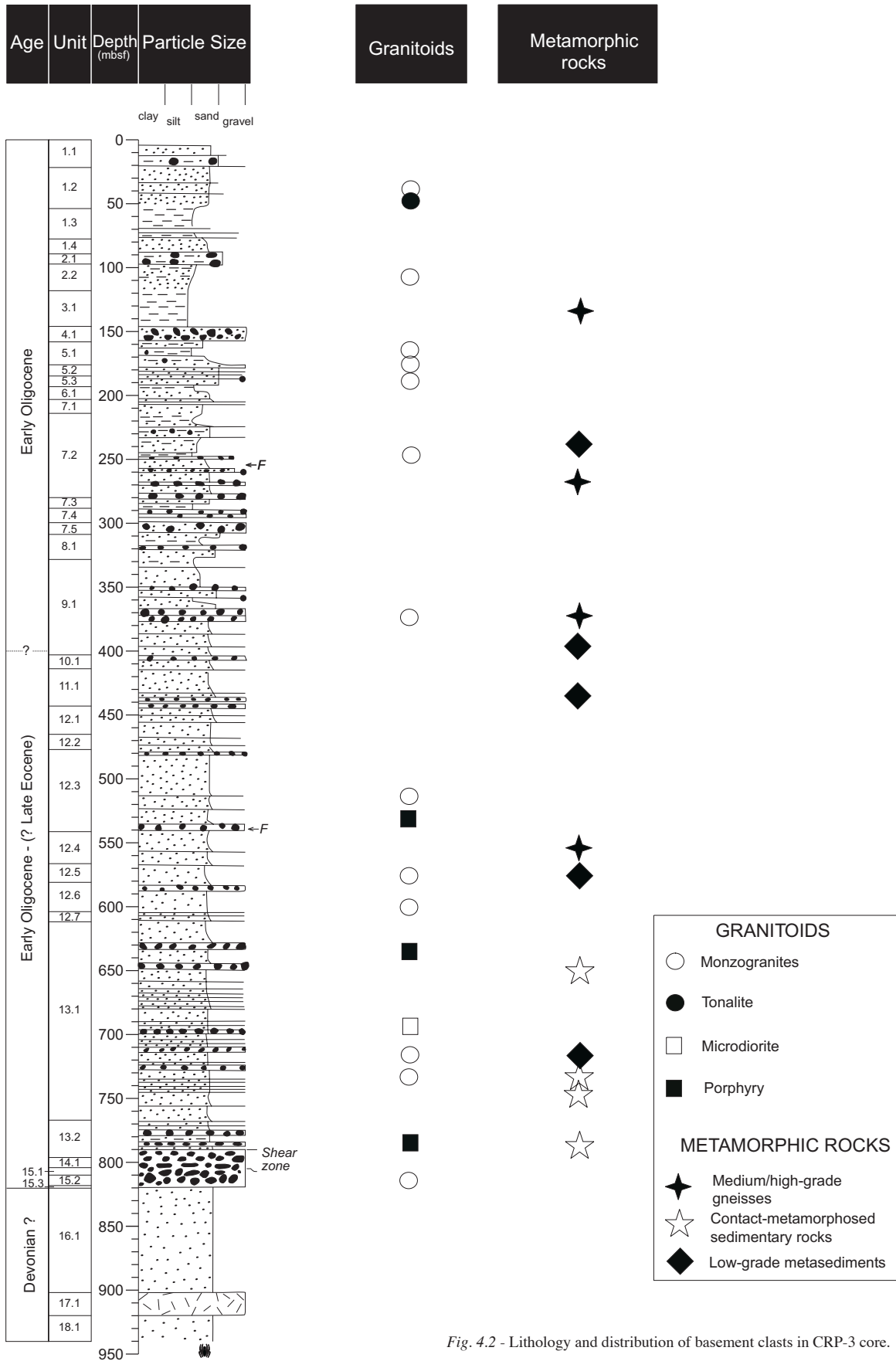


Fig. 4.2 - Lithology and distribution of basement clasts in CRP-3 core.

Tab. 4.1 - Basement clasts in Cenozoic sedimentary strata recovered by CRP-3 drillhole: list of sampled clasts and preliminary petrographical data. Note: lithostratigraphical unit designation follows figure 3B-1 of section on Description of Sequence. Mineral abbreviations according to Kretz (1983). G.H.I.C.: Granite Harbour Igneous Complex; K.G.: Koettlitz Group; B.S.: Beacon Supergroup; S.G.: Skelton Group.

Sample code	Box	Top (mbsf)	Bottom (mbsf)	Lithology	Main petrographical features	Inferred provenance	LU
TAL2	8	30,61	30,63	grey Bt-bearing monzogranite	equigranular (fine-grained), hypidiomorphic	G.H.I.C.	1,2
TAL4	13	43,57	43,58	pink Bt-Hbl bearing monzogranite	equigranular (medium-grained), hypidiomorphic	G.H.I.C.	1,2
TAL5	15	50,25	50,27	Act-bearing leucotonalite	heterogranular (fine- to medium-grained), hypidiomorphic, altered	G.H.I.C.	1,2
TAL11	34	107,32	107,36	Bt-bearing leucomonzogranite	heterogranular (fine- to medium-grained), hypidiomorphic, slightly foliated fabric, strongly altered	G.H.I.C.	2,2
TAL16	42	132,19	132,21	Ms-Tur bearing quartzite	equigranular (fine-grained), subpolygonal granoblastic texture, slightly foliated	K.G.	3,1
TAL22	53	166,18	166,20	mylonitic Grt-Bt leuco-orthogneiss	heterogranular (fine- to medium-grained), gneissic texture (mm-scale compositional layering) with mm-sized feldspar porphyroclasts	K.G.	5,1
TAL23	54	168,73	168,79	Bt-bearing monzogranite	inequigranular (fine- to coarse-grained), hypidiomorphic, slightly altered	G.H.I.C.	5,1
TAL26	57	176,03	176,09	pink Bt-Hbl monzogranite	inequigranular (fine- to coarse-grained), porphyritic, mm-sized feldspar phenocrysts and fine-grained allotriomorphic groundmass	G.H.I.C.	5,2
TAL27	57	178,41	178,44	pink Bt-Hbl monzogranite	equigranular (medium-grained), hypidiomorphic, altered	G.H.I.C.	5,3
TAL36	70	216,98	217,24	grey Bt-bearing leucomonzogranite	inequigranular (fine- to medium-grained), hypidiomorphic, sub-solidus deformational microstructures, altered	G.H.I.C.	7,2
TAL41	74	227,98	228,01	Bt-bearing meta-quartz arenite	equigranular (fine-grained), interlobate granoblastic	B.S.? (contact metamorphosed?)	7,2
TAL42	75	231,78	238,80	mylonitic Bt leuco-orthogneiss	heterogranular (fine- to medium-grained), gneissic texture (mm-scale compositional layering) with mm-sized feldspar porphyroclasts	K.G.	7,2
TAL43	83	256,38	256,40	pink Bt-Hbl monzogranite	inequigranular (fine- to medium-grained), hypidiomorphic, altered	G.H.I.C.	7,2
TAL57	109	335,31	335,35	pink Bt-Hbl monzogranite	inequigranular (fine- to medium-grained), hypidiomorphic, altered	G.H.I.C.	9,1
TAL58	109	337,19	337,23	a) Hbl-bearing Bt orthogneiss; b) Bt-bearing metasiltstone	a) heterogranular (fine- to medium-grained), gneissic texture (mm-scale compositional layering) with ribbon-like quartz aggregates; b) very fine-grained to fine-grained, grain size and compositional layering, Bt and Opm spots	a) K.G. b) B.S.? (contact metamorphosed?)	9,1
TAL59	110	337,57	337,61	Gph-bearing marble	inequigranular (fine- to medium-grained), grain size layering, interlobate granoblastic	K.G.	9,1
TAL62	118	370,24	370,27	grey Bt-bearing granite	equigranular (medium-grained), hypidiomorphic	G.H.I.C.	9,1
TAL75	135	442,79	442,83	Bt-bearing meta-quartz arenite	fine-grained, Bt spots	B.S.? (contact metamorphosed?)	11,1
TAL78	145	482,52	482,54	grey Bt granite	equigranular (medium-grained), hypidiomorphic	G.H.I.C.	12,3
TAL79	146	488,61	488,63	grey Bt granite	equigranular (medium-grained), hypidiomorphic	G.H.I.C.	12,3
TAL82	157	536,60	536,62	red porphyry	mafic and feldspar phenocrysts set within a very fine-grained altered groundmass	G.H.I.C.?	12,3
TAL83	161	554,70	554,76	Sil-Bt paragneiss	fine-grained, compositional layering, granolepidoblastic	K.G.	12,4
TAL84	163	561,54	561,58	black Czo/Ep-Cal-Bt metasiltstone	very fine-grained, compositional layering, interlobate granoblastic	B.S.? (contact metamorphosed?)	12,5
TAL85	163	561,91	561,97	pink Bt monzogranite	equigranular (fine-grained), hypidiomorphic	G.H.I.C.	12,5
TAL92	173	605,77	605,80	Bt-Ms leucogranite	equigranular (fine-grained), hypidiomorphic	G.H.I.C.	12,6
TAL96	179	627,17	627,20	dark grey porphyry	feldspar phenocrysts set within a very fine-grained altered groundmass	G.H.I.C.?	13,1
TAL97	179	628,06	628,08	foliated Bt leucomonzogranite	heterogranular (fine- to medium-grained), gneissic texture with mm-sized feldspar porphyroclasts and quartz ribbons	G.H.I.C.	13,1
TAL98	179	628,69	628,71	Cal-Bt schist	very fine-grained, compositional layering, lepidogranoblastic	S.G.? /B.S.? (contact metamorphosed?)	13,1
TAL99	182	641,50	641,52	Bt-Hbl microdiorite	equigranular (fine-grained), hypidiomorphic/sub-ophitic	G.H.I.C.	13,1
TAL100	182	644,50	644,52	Bt orthogneiss	heterogranular (fine- to medium-grained), interlobate granoblastic and quartz ribbons	G.H.I.C./K.G.?	13,1
TAL103	190	675,63	675,65	grey Bt-bearing monzogranite	inequigranular (fine- to medium-grained), hypidiomorphic, sub-solidus deformational microstructures	G.H.I.C.	13,1
TAL109	199	713,29	713,31	Bt-Hbl monzogranite	equigranular (medium-grained), hypidiomorphic, altered	G.H.I.C.	13,1
TAL110	205	734,67	734,71	Leyerd Bt-Cam-Qtz metamarl	very fine- to fine grained, compositional and grain size layering, granoblastic Cal-rich layers, lepidogranoblastic Bt-rich layers	S.G.? /B.S.? (contact metamorphosed?)	13,1
TAL112	206	738,45	738,48	pink Bt-Hbl granite	equigranular (coarse-grained), hypidiomorphic, altered	G.H.I.C.	13,1
TAL113	210	756,16	756,19	Cal-Cam-Bt meta-feldsarenite	very fine-grained, compositional layering, interlobate lepidogranoblastic	S.G.? /B.S.? (contact metamorphosed?)	13,1
TAL118	215	774,96	774,99	Bt meta-sandstone	very fine-grained, compositional layering, interlobate lepidogranoblastic	S.G.? /B.S.? (contact metamorphosed?)	13,2
TAL119	217	781,93	781,97	Bt meta-sandstone	very fine-grained, compositional layering, interlobate lepidogranoblastic	S.G.? /B.S.? (contact metamorphosed?)	13,2
TAL121	218	785,56	785,63	light grey porphyry	feldspar phenocrysts set within a very fine-grained altered groundmass	G.H.I.C.?	13,2
TAL125	225	815,23	815,25	grey Bt granite	equigranular (medium-grained), hypidiomorphic	G.H.I.C.	15,2

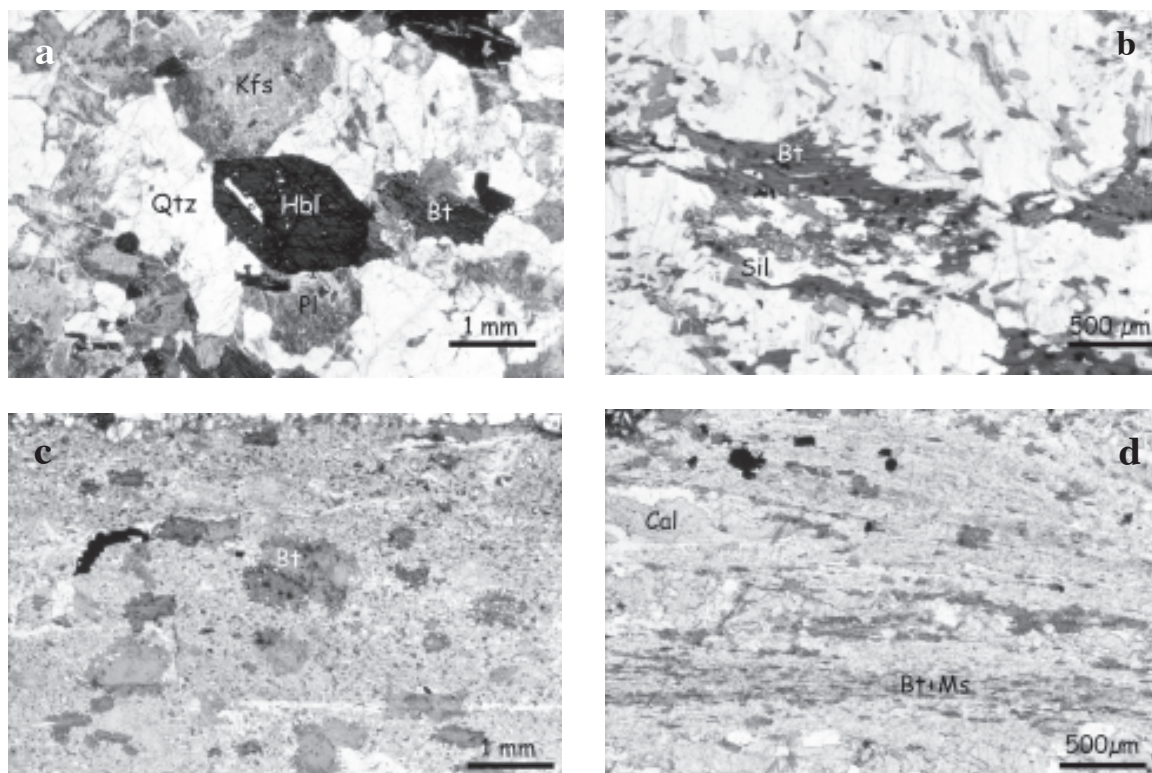


Fig. 4.3 - Photomicrographs of the principal basement rock types in CRP-3 core. a) Pink biotite-hornblende granite (738.45 mbsf), hypidiomorphic texture with altered alkali feldspar (Kfs) phenocrysts, saussuritized plagioclase (Pl), chloritized biotite flakes (Bt) and interstitial quartz (Qtz); b) □sillimanite-biotite paragneiss (554.70 mbsf): the foliation is defined by the preferential dimensional orientation of biotite and sillimanite, matrix minerals include K-feldspar, plagioclase and quartz; c) contact-metamorphosed metasilstone (561.54 mbsf): randomly oriented flakes of biotite indicate a static recrystallization typical of low-grade contact metasedimentary rocks; d) calcite-bearing biotite schist (628.69 mbsf): the foliation is defined by biotite and muscovite fine-grained lepidoblasts.

spectrum of metamorphic conditions. Orthogneisses, sillimanite-biotite paragneiss (Fig. 4.3) and marble show mineral assemblages and microstructures consistent with upper amphibolite-facies regional metamorphic conditions. In contrast, meta-quartz arenite and metasilstone are characterised by mineral assemblages indicative of biotite-zone (low-grade) conditions, with either decussate, spotted microstructures diagnostic of contact metamorphism, or oriented fabrics indicative of syn-tectonic recrystallizations, most likely related to regional metamorphism (Fig. 4.3).

PROVENANCE

Preliminary petrographical investigations indicate that several basement lithologies were involved as sources of basement clasts in the Cenozoic sedimentary strata recovered in the CRP-3 drillhole. As in CRP-1 and CRP-2/2A (Talarico & Sandroni, 1998; Talarico et al., in press), most of the basement pebbles were supplied by source-rock units belonging to the Cambro-Ordovician Granite Harbour Igneous Complex, which is the dominant component in the local basement (Gunn & Warren,

1962; Allibone et al., 1993a, 1993b). Like CRP-1 and CRP-2/2A, the ubiquitous occurrence of undeformed biotite±hornblende monzogranite pebbles throughout the cored interval apparently reflects the dominance of these lithologies in the onshore basement. Preliminary data concerning the other, less common and impersistent, granitoid varieties are also consistent with a local provenance.

Metamorphic rocks such as biotite-sillimanite paragneiss and biotite-garnet orthogneiss are also known to be a common metasedimentary lithologic type in the amphibolite-facies Koettlitz Group south of Mackay Glacier (Grindley & Warren, 1964; Williams et al., 1971; Findlay et al., 1984; Allibone, 1992; Turnbull et al., 1994). Petrographically similar orthogneiss types were also found in CRP-1 and in CRP-2/2A. CRP-3 is apparently devoid of Ca-silicate rocks, which were found to be relatively common in the two previous CRP drillholes. In contrast, clasts of contact-metamorphosed terrigenous-sedimentary rocks and of foliated low-grade metasediments are rather abundant, even if scattered throughout the core below c. 228 mbsf.

The occurrence of low-grade metasandstone showing

foliated fabrics is noteworthy as the onshore exposures of these rocks are very limited and restricted to areas between the Skelton and Koettlitz Glaciers, about 200 km south of the CRP-3 drillsite (Skelton Group; Grindley & Warren, 1964).

The provenance and primary geological setting of contact-metamorphosed sedimentary rocks remain uncertain. Apart from the thermal-metamorphic overprint, these rocks show a broad lithological and petrographical similarity with comparable rock types occurring in the Beacon Supergroup. In such case, the contact-metamorphic overprint could be related to thermal and hydrothermal processes which accompanied the emplacement and cooling of Ferrar Supergroup intrusive and sub-volcanic suites. However, a provenance from presently unknown post-Jurassic (?Paleogene) sedimentary sequences deposited on down-faulted blocks within the Victoria Land Basin cannot be excluded.

VOLCANIC CLASTS

METHODS

We studied volcanic material in CRP-3 at two different scales. Volcanic clasts, with sizes ranging from granule to boulder, were investigated by classical petrographical methods, including thin-section examination. Sand to silt fractions were also collected regularly and analysed by means of smear slides for the presence of glass shards, in order to record the volcanic activity coeval with the deposition.

Both coarse- and fine-grained materials were sampled for further geochemical and mineralogical analyses.

VOLCANIC CLASTS

Volcanic clasts are medium- to fine-grained black to grey mafic rocks. Their shape varies from subangular to subrounded. They are generally massive, although vesicular fragments with vesicles filled with secondary minerals are also common. The abundance of vesicular clasts seems to increase downcore.

All the sampled clasts share the same mineral assemblage: major minerals are plagioclase and clinopyroxene, whereas pigeonite, K-feldspar, orthopyroxene and quartz are also found in most of the specimens. Ilmenite and magnetite are ubiquitous accessory minerals. Alteration is significant and affects mainly pyroxenes and the groundmass. Clasts in which the original mineral assemblage is totally replaced by secondary minerals are uncommon.

The above mineral assemblage is known to be typical of the Ferrar Supergroup rocks that display a subalkaline affinity and have a Jurassic age (Elliot et al., 1995; Kyle, 1999). These rocks crop out as sills (Ferrar dolerite), lava flows (Kirkpatrick flows), and pyroclastic deposits (Mawson Formation, Kirkpatrick Basalt pyroclasts) (Fig. 4.4)



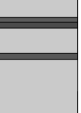

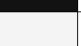


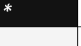







Age (Ma)	Strat. Rel.	Geological Units
c. 24-0		<i>M^cMurdo Volcanic Group</i> (lavas, tephra, etc) South Victoria Land
c. 48-0		<i>M^cMurdo Volcanic Group</i> (lavas, tephra, plutons) North Victoria Land
c. 180		<i>Kirkpatrick Basalt</i> (flows with intercalated pillows, tuffs, tuffites, and volcanic sandstones) (Ferrar Supergroup)
c. 180		<i>Mawson Fm.</i> Ferrar Supergroup
Victoria Group c. 280-200 * c. 190-160		<i>Ferrar Supergroup</i> (sill)
		<i>Beacon Supergroup</i> (sandstones)
		<i>Ferrar Supergroup</i> (sill)
		<i>Beacon Supergroup</i> (sandstones)
		<i>Beacon Supergroup</i> (sandstones)
Taylor Group c. 415-350 * c. 190-160		<i>Ferrar Supergroup</i> (sill)
		<i>Beacon Supergroup</i> (sandstones)
		<i>Ferrar Supergroup</i> (peneplain sill)
c. 540-470 * c. 190-160		<i>GHIC-KG</i>
		<i>Ferrar Supergroup</i> (basement sill)
		<i>GHIC-KG</i>

Fig. 4.4 - Schematic stratigraphical relationships for rocks cropping out in southern Victoria Land. Ages from Elliot et al. (1986), Roland & Worner (1996), McIntosh (in press), Turnbull et al. (1994). GHIC: Granite Harbour Igneous Complex, KG: Koettlitz Group.

throughout the Transantarctic Mountains. Consequently, rocks of the Ferrar Supergroup could be the main source of volcanic detritus in CRP-3. Fragments showing a mineral assemblage (olivine, alkali pyroxene or amphibole) typical of the McMurdo volcanic group (M^cMVG) (Cape Roberts Science Team, 1998b) are not represented in any of the CRP-3 specimens.

Textural and grain-size features observed in thin sections enabled us to divide all the sampled clasts into three groups. Table 4.2 gives a list of the sampled clasts, core depth and group attribution. The number of clasts in each different group does not reflect the relative abundance of these clasts in the core.

Group I consists of medium to fine-grained holocrystalline rocks, with subophitic texture (Fig. 4.5a). Plagioclase is the most abundant phase, forming

subhedral crystals (maximum length = 2 mm); Composition, estimated by optical methods, varies from oligoclase to labradorite. In some crystals, sericite extensively replaces crystals. Augitic clinopyroxene is subordinate and forms subhedral and anhedral crystals (maximum length = 4 mm); in most samples it is largely altered to smectites. Pigeonite is minor as well and appears associated with clinopyroxene as subhedral crystals. Both rhombohedral and cubic Fe-Ti oxide are present in most samples. Less frequently, only acicular ilmenite crystals with a leucoxene coating are found. In most samples, fine-grained quartzo-feldspathic intergrowths are visible in interstices between plagioclase and pyroxene crystals.

In fine-grained clasts plagioclase is euhedral, pyroxenes tend to be acicular and a very fine-grained cryptocrystalline matrix is quite often deeply altered to sericite and clay minerals.

Group II is made-up of medium- to fine-grained hypocrySTALLINE rocks with textures varying from intergranular to intersertal (Fig. 4.5b). We can consider these rocks aphyric, since crystal sizes are almost constant. Plagioclase is the most abundant phase and forms a complex network of acicular crystals with pyroxene. The composition of plagioclase ranges from oligoclase to labradorite. Clinopyroxene crystals are rarely preserved, being frequently transformed to smectite. Sometimes relics of the original clinopyroxene are preserved only at the core of the large prismatic crystals. Pigeonite is rare, while orthopyroxene occurs as single-prismatic, euhedral crystals. Anhedral quartz is present as discontinuous segregations. The interstitial material ranges from very fine-grained cryptocrystalline matrix, in which Fe-Ti oxides and pyroxene microlites replaced by smectites are barely recognisable, to a very rare, palagonitised brown glass that embodies tiny plagioclase and pyroxene aggregates. Group II clasts are generally non-vesicular, even though we detected some irregularly shaped vesicles filled by secondary minerals (carbonate, chalcedony, cristobalite, zeolites).

Group III includes aphyric and weakly porphyritic clasts, generally hypocrySTALLINE with rare holohyaline terms. These rocks show a low vesicularity, even though in some specimens amygdaloids filled with secondary minerals form as much as 30% of the rocks (Fig. 4.5c). In these clasts we observed few hypidiomorphic andesine to labradoritic plagioclase and augitic clinopyroxene phenocrysts. Sometimes anhedral quartz forms discontinuous segregations (c. 1 mm across), but more than 90% of the rock comprises a quenched matrix (Fig. 4.5d) consisting of acicular crystals of plagioclase and feathery microlites of clinopyroxene. These are arranged as a felt-like network, whose interstices are occupied by blocky Fe-Ti oxides, cryptocrystalline clay-altered material, and more rarely, brown palagonitic glass. In the more vesiculated, scoriaceous clasts, portions with clear brown glass without microlites become predominant.

Tab. 4.2 - Main textural characters, sizes and group attribution of volcanic clasts in CRP-3.

Depth (mbsf)	Clast size (cm)	Crystallinity - Texture	Grain size	Group
5.93	nd	holocrystalline, subophitic	medium	I
6.66	nd	holocrystalline, subophitic	medium-fine	I
9.44	nd	holocrystalline, subophitic	medium-fine	I
33.60	8	holocrystalline, subophitic	medium-fine	I
42.70	nd	holocrystalline, subophitic	medium-fine	I
47.46	nd	holocrystalline, subophitic	medium-fine	I
70.09	2	holocrystalline, subophitic	medium	I
73.86	1	hypocrystalline, variolitic	very fine	III
73.90	1	hypocrystalline, intersertal	fine	II
91.18	>4	holocrystalline, subophitic	fine	I
105.39	1.5	hypocrystalline, variolitic	very fine	III
149.70	3.5	hypocrystalline, intersertal	fine	II
150.08	0.5	hypocrystalline, intergranular	medium	II
151.43	3	hypocrystalline, variolitic	very fine	III
163.26	>2	glassy, amygdaloid, palagonitic		III
165.91	1.5	holocrystalline, subophitic	medium	I
178.77	2.5	hypocrystalline, intersertal	fine	II
178.79	1.5	hypocrystalline, intergranular	fine	II
182.26	<1	hypocrystalline, intergranular	fine	II
183.91	4	hypocrystalline, intergranular	fine	II
184.34	4	hypocrystalline, intersertal	fine	II
208.88	<.5	hypocrystalline, intergranular	medium	II
235.97	2	hypocrystalline, intergranular	medium	II
248.70	1.5	holocrystalline, subophitic	fine	I
251.52	1.5	holocrystalline, subophitic, altered	fine	I
263.11	15	holocrystalline, subophitic	fine	I
264.34	1.5	holocrystalline, subophitic	medium-fine	I
292.04	>3	holocrystalline, subophitic	medium-fine	I
306.59	1	glassy, amygdaloid, palagonitic		III
307.91	>3	hypocrystalline, intergranular	medium	II
313.96	>4	hypocrystalline, intergranular	medium	II
328.40	nd	holocrystalline, subophitic, altered	fine	I
337.34	nd	holocrystalline, subophitic	fine	I
344.61	4	holocrystalline, subophitic, altered	medium-fine	I
369.91	<1	holocrystalline, subophitic	medium	I
370.18	2	hypocrystalline, hyalopilitic	very fine	III
372.50	>4	hypocrystalline, intergranular	fine	II
375.76	>4	holocrystalline, subophitic	medium	I
377.46	<1	holocrystalline, subophitic	medium-fine	I
377.70	>5	holocrystalline, subophitic	medium-fine	I
386.83	<1	hypocrystalline, intergranular	medium	II
387.05	4	hypocrystalline, intergranular	medium	II
414.15	1.5	hypocrystalline, variolitic, amygdaloid	very fine	III
415.43	1.5	holocrystalline, subophitic	medium-fine	I
423.32	1	holocrystalline, subophitic	fine	I
439.23	<1	holocrystalline, subophitic	medium	I
441.85	1.5	hypocrystalline, variolitic	very fine	III
450.49	4.5	hypocrystalline, intergranular	fine	II
462.76	0.6	holocrystalline, subophitic	fine	I
464.71	2.5	hypocrystalline, intergranular, vesicular	medium	II
469.24	4	hypocrystalline, variolitic, amygdaloid	very fine	III
479.03	<1.5	hypocrystalline, intergranular	fine	II
480.55	1	glassy, palagonitic		III
495.46	3	holocrystalline, subophitic	medium	I
516.71	4	hypocrystalline, intergranular	fine	II
544.37	4	hypocrystalline, hyalopilitic	very fine	III
548.30	1	holocrystalline, subophitic	medium-fine	I
562.13	2	hypocrystalline, variolitic, amygdaloid	very fine	III
568.26	1.5	hypocrystalline, variolitic, amygdaloid	very fine	III
570.54	2.5	glassy, palagonitic		III
578.16	2	holocrystalline, subophitic	fine	I
580.34	<1	hypocrystalline, variolitic, amygdaloid	very fine	III
593.28	2	holocrystalline, subophitic	medium	I
605.33	1	holocrystalline, subophitic	fine	I
625.08	2	hypocrystalline, intergranular, vesicular	fine	II
627.11	>4	hypocrystalline, variolitic	very fine	III
635.89	2	hypocrystalline, intergranular	fine	II
653.66	1.5	glassy, amygdaloid		III
665.09	1.5	holocrystalline, subophitic	medium	I
671.44	2	holocrystalline, subophitic	fine	I
683.64	1.5	holocrystalline, subophitic	medium	I
690.40	3.5	glassy, amygdaloid, palagonitic		III
727.61	3	hypocrystalline, intersertal, vesicular	fine	II
735.01	1.5	hypocrystalline, intersertal, vesicular	fine	II
738.71	1	holocrystalline, subophitic	fine	I
769.30	3	holocrystalline, subophitic	fine	I
788.20	>4	holocrystalline, subophitic	fine	I
789.59	2.5	hypocrystalline, intersertal	fine	II

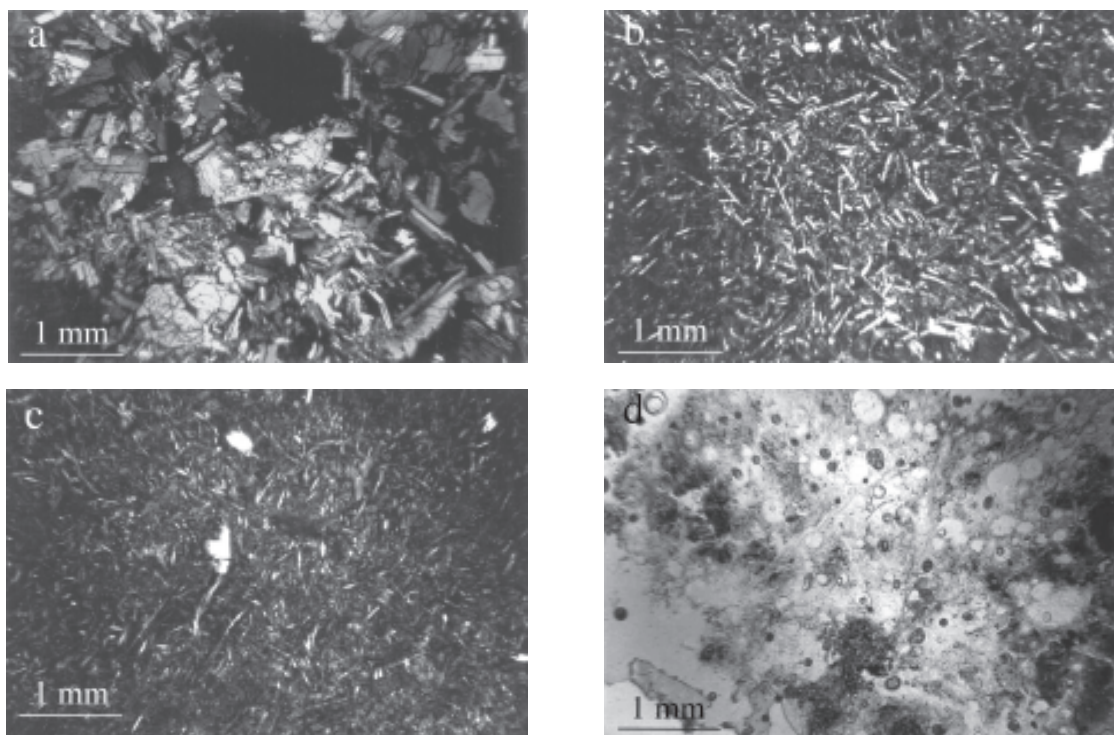


Fig. 4.5 - Photomicrograph of CRP-3 selected clasts; a) medium-grained group I clast with subophitic texture; b) medium-grained group II clast showing acicular plagioclase and clinopyroxene and intergranular texture; c) amygdaloid texture in a vesicular glassy clast of group III; d) plagioclase phenocryst and quenched crystals in a clast from group III.

PRELIMINARY CONCLUSIONS ON VOLCANIC-CLAST PROVENANCE

The above textural differences are related to cooling rate and perhaps to different emplacement mechanisms. Subophitic textures are typical of intrusive magmatic bodies as sills, but may be found as well in the inner portions of thick lava flows that undergo a very slow cooling. Intersertal to intergranular textures, with a variable abundance of interstitial glass, are quite common in lava flows or can be found in the external portions of dykes and sills. Glass-rich volcanics and quenched crystals indicate a high cooling rate, such as for those associated with magma chilled by contact with water or country rocks.

Hence, we can use textural characteristics of the clasts to infer their possible relationship with Ferrar Supergroup outcrops on land. As a matter of fact, clasts of group I showing subophitic textures should have been derived by the erosion of Ferrar sills that intrude the basement and Beacon sedimentary cover at different levels (Fig. 4.4).

Clasts of group II could represent the external part of these sills, but more probably they are eroded fragments of the Kirkpatrick lava flows. It is worth noting the close correspondence among some CRP-3 clasts, that show distinctive single orthopyroxene crystals, and the Mount Fazio Chemical Type (MFCT) lavas described in Mesa

Range by Elliot et al. (1995), that display this similar but unusual character. The MFCT lavas are thought to occur in the lower part of the Kirkpatrick volcanic succession.

Clasts of group III possibly derive from the external portions of the Kirkpatrick lava flows. Features observed in the least vesicular clasts belonging to this group seem to match those of Scarab Peak chemical type rocks (SPCT) that, following Elliot et al. (1995), cap the Kirkpatrick succession in the Mesa Range area. Alternatively, glassy portions could be pillow-lavas fragments derived from the middle part of the Kirkpatrick group (discrete horizons between lava flows; Roland & Worner, 1996). Finally, the glassy scoriaceous clasts may be derived from pyroclastic or volcanoclastic deposits that form the lower part of the Kirkpatrick succession (Fig. 4.4, Kirkpatrick Basalt pyroclasts, Mawson and Exposure Hill Formations) (Elliot et al., 1986).

GLASS SHARDS

A very small number of volcanic glass shards was detected in smear slides of most of the sand-silt fractions of CRP-3 (Tab. 4.3). They are very scant (maximum of 10 shard per smear slide), display angular to subangular shapes and have sizes ranging from 30 to 200 μm . Small grain size, flake-like shapes and very low abundance impede easy recognition and an accurate evaluation of

modal abundance in thin sections (see section on Sand Mineralogy).

The more abundant type is brown to light brown glass (sideromelane); colourless and light-green (evolved?) varieties are less common. Most of them appear to be fresh; palagonite and clay-mineral alteration are uncommon. Some glass shards embody small opaque grains (Fe-Ti oxides?) or feldspar fragments, whereas vesicles are rare.

On the whole, glass fragments found in CRP-3 show petrographical features similar to those found in CRP 2-2/A, where lapilli and glass shards, with alkaline compositions typical of M^cMVG rocks, were found above 320 mbsf. However, size and abundance of glass fragments at CRP-3 are significantly different from those of the upper portion of CRP2/2A: these instead match the pattern found in the lower section of the same site (below 320 mbsf), where glass shards are almost absent and magmatic affinities are still undefined. Nevertheless, since the compositional data, which remain the critical discriminating factor to indirectly infer the age of the volcanism, are not available for CRP-3 glass shards, hypotheses on their origin could still be formulated on the basis of textures, size, and abundance. The small size of the glass shards and their scarcity indicate a distant source, whatever their origin. If the shards are a distal air-fall deposit, the alkaline volcanism, active in northern Victoria Land since 48 Ma (Tonarini et al., 1997), can be postulated as a possible source. Conversely, since shards show low or no vesiculation and their outlines seem mainly controlled by fracture surfaces rather than by broken bubble walls, an origin by fragmentation processes driven by a violent water/ice-magma interaction can alternatively be inferred. In this case glass shards may indicate volcanic activity coeval with deposition in which external water is involved (subglacial eruptions?) or may represent erosion and reworking of older phreatomagmatic deposits interlayered with the Kirkpatrick succession (Elliot et al., 1986).

SEDIMENTARY CLASTS

We present here a preliminary petrographical investigation on selected sedimentary-clast samples from CRP-3. In terms of grain size, all specimens studied belong to the pebble group. They can vary from rounded to subangular. We recognised six principal lithological categories: quartzarenite, feldspathic arenite, feldspathic wacke, siltstone, claystone and coal clasts. The majority of the clasts belong to the quartzo-feldspathic group. The main petrographical features are summarized as follows:

1) Quartzarenites. These consist of moderately sorted sandstone. Quartz grains vary from coarse to medium in size and from rounded to well rounded in shape. Grains are compositionally represented mainly by quartz, some of which have small inclusions; minor

components are fine-grained fragments of altered plagioclase, potassium feldspar, and metamorphic-rock fragments. The cement around the detrital quartz grains consists of a well developed phase of authigenic quartz overgrowth, with the grain surface often marked by a thin layer of inclusions (probably iron oxides). Locally, some interstitial clay/silt matrix is present, mainly mica derived from plagioclase alteration.

- 2) Feldspathic arenites. These consist of very poorly sorted sandstone. Grains vary in size from fine to medium and from angular to subrounded in shape. The clay component is dispersed throughout the matrix, together with silt particles. Grains are dominantly represented by quartz; other components are potassium feldspar and plagioclase (altered in carbonate and micas). Lithic fragments of dolerite and basement rocks are common. Both biotite and muscovite flakes are present and show deformation and kink structures. Intergrowths of chlorite and muscovite in the form of rosette-shaped clusters of plate-like crystals (possibly from the alteration of plagioclase) are present in some specimens, either attached to detrital quartz grains or as growths in the pore voids.
- 3) Feldspathic wackes. These consist of very poorly sorted sandstone. Grains vary in size from fine to very fine and from angular to very angular in shape. Grains are dominantly represented by quartz; other components are potassium feldspar and plagioclase (often altered to carbonate and micas). Lithic fragments of dolerite and basement rocks are also present. The matrix is represented by abundant clay components, which in cases can become dominant in percentage. Silt particles are also common.
- 4) Siltstones. These are represented by dominant silt-sized grains, mainly subangular to angular in shape and within a clay matrix. Quartz and plagioclase grains are also present, ranging in size from fine- to very fine-grained. Plagioclase grains show a variable degree of alteration to mica. Metamorphic rock fragments may also be present.
- 5) Claystones. These are represented by an unresolvable clay matrix. The sand- and silt-sized detrital component is characterized by quartz grains (from very fine to medium size) and rare plagioclase grains, many of which show a diffuse alteration to micas and carbonate. In some, cases a thin isopachous carbonate rim surrounds the quartz grains.
- 6) Coal fragments. These can vary in size from granules to pebbles and, in shape, from subrounded to angular. The majority of the specimens have a detrital origin, but a few have a flakey appearance. At the macroscopic level they appear to still be un lithified, suggesting an *in-situ* coalification process at a shallow burial depth. The detrital coal clasts commonly show an amorphous microstructure; in some cases, microfractures and cracks (possibly induced by dessication or compression) filled by clay components are present. Detrital components

Tab. 4.3 - Occurrence and estimated abundance of glass shards in CRP-3.

Depth (mbsf)	LSU	Grain size	Abundance	Type	Dim. (mm)
3,00	1,1	diamictite	x	brown	0,10
6,00	1,1	diamictite	xx	brown	0,20
9,40	1,1	diamictite	x	brown	0,05
9,86	1,1	diamictite	x	brown	0,06
16,10	1,1	diamictite	xx	brown	0,20
16,75	1,2	muddy sandstone	x	brown	0,05
32,55	1,2	muddy sandstone	x	brown	0,05
33,14	1,2	muddy sandstone	x	brown	0,15
49,40	1,2	muddy sandstone	x	brown	0,05
155,45	4,1	fine sandstone	x	brown	0,15
155,55	4,1	fine sandstone	x	brown	0,05
155,91	4,1	fine sandstone	r-?	brown	
155,93	4,1	fine sandstone	x	brown	0,05
157,79	5,1	sandy siltstone	a		
172,96	5,2	muddy sandy pebble conglomerate	r-?	brown	
177,17	5,3	medium sandstone	r-?	brown	
179,39	5,3	sandy siltstone and very fine and fine sandstone	x	brown	0,05
181,28	5,3	sandy siltstone and very fine and fine sandstone	x	brown	0,05
185,13	6,1	muddy fine grained sandstone	x	brown, green	0,07
187,05	6,1	muddy fine grained sandstone	a		
187,07	6,1	muddy fine grained sandstone	a		
189,21	6,1	siltstone	a		
189,21	6,1	siltstone	a		
190,17	6,1	muddy very fine sandstone	xx	colourless, brown	0,10
190,33	6,1	muddy very fine sandstone	x	brown	0,07
192,84	6,1	muddy very fine sandstone	xx	colourless, brown	0,10
193,97	6,1	muddy very fine sandstone	r-?	brown	
195,84	6,1	muddy very fine sandstone	x	colourless	0,10
196,04	6,1	muddy very fine sandstone	a		
200,71	6,1	muddy very fine sandstone	a		
201,13	6,1	muddy very fine sandstone	a		
201,97	6,1	muddy very fine sandstone	a		
230,00	7,2	fine sandstone	x	brown	0,05
234,67	7,2	medium sandstone	x	brown	0,05
239,19	7,2	medium sandstone	x	brown	0,05
242,30	7,2	siltstone	x	brown	0,05
289,99	7,4	pebble boulder conglomerate	x	brown	0,05
310,50	8,1	muddy fine sandstone	x	brown	0,05
311,00	8,1	muddy fine sandstone	x	brown	0,05
320,60	8,1	sandy siltstone	r-?	brown, colourless	
321,50	8,1	sandy siltstone	xx	brown, colourless	0,05
333,22	9,1	sandstone fine	x	brown	0,05
364,10	9,1	medium to fine sandstone	a		
373,84	9,1	medium to fine sandstone	xx	brown, colourless	0,30
384,70	9,1	medium to fine sandstone	x	brown	0,10
385,30	9,1	medium to fine sandstone	a	brown	
391,00	9,1	medium to fine sandstone	r-?	brown	
398,50	9,1	medium to fine sandstone	a		
401,84	9,1	medium to fine sandstone	r-?	colourless	
405,80	9,1	medium to fine sandstone	r-?	colourless, green	
406,23	10,1	sandy siltstone	x	colourless, brown	0,05
408,65	10,1	sandy siltstone	x	colourless, brown	0,05
413,07	10,1	siltstone	xx	brown, green	0,10
419,90	11,1	medium to fine sandstone	n		
423,21	11,1	medium to fine sandstone	n		
423,26	11,1	medium to fine sandstone	r-?	green	
428,80	11,1	coarse to fine sandstone	r-?	brown, colourless	
436,06	11,1	coarse to fine sandstone	x	brown	0,10
439,90	11,1	medium sandstone	r-?	brown, green	
440,26	11,1	medium sandstone	x	brown	0,10
443,03	11,1	pebble to cobble conglomerate	x	brown, lighth, green	0,05
475,77	12,3	fine sandstone	a		
480,51	12,3	muddy sandstone fine to coarse	a		
480,67	12,3	muddy sandstone fine to coarse	x	brown	0,05
480,72	12,3	muddy sandstone fine to coarse	a		
481,13	12,3	muddy sandstone fine to coarse	r-?	brown	
481,70	12,3	fine to coarse sandstone	a		
483,78	12,3	fine to coarse sandstone	a		
486,03	12,3	fine to coarse sandstone	x	brown	0,10
489,75	12,3	fine to coarse sandstone	a		

a: absent, r-?: very rare or dubious, x: <5 per smear slide, xx:>5 per smear slide

Grain size as reported in core log

Tab. 4.3 - Continued

Depth (mbsf)	LSU	Grain size	Abundance	Type	Dim. (mm)
490,50	12,3	fine to coarse sandstone	a		
500,80	12,3	sandstone	r-?	brown	
501,00	12,3	sandstone	r-?	colourless, vesicular	
510,10	12,3	fine to medium sandstone	a		
518,20	12,3	fine to medium sandstone	a		
522,99	12,3	muddy sandstone very fine	x	brown, colourless	0,05
527,09	12,3	very fine sandstone	r-?	brown	
539,70	12,4	pebbly medium grained sandstone	r-?	brown	
543,00	12,4	fine sandstone	xx	brown	0,10
543,01	12,4	fine sandstone	a		
544,05	12,4	fine sandstone	a		
544,71	12,4	fine sandstone	a		
546,98	12,4	fine sandstone	a		
550,95	12,4	fine sandstone	x	light brown	0,05
554,60	12,4	fine sandstone	a		
560,22	12,5	sandstone	a		
560,60	12,5	sandstone	a	brown, vesicular	
561,60	12,5	sandstone	a		
569,42	12,5	sandstone	a		
581,82	12,6	sandstone	x	brown	0,05
581,98	12,6	sandstone	x	brown	0,05
585,75	12,6	sandstone	a		
590,00	12,6	sandstone	a		
596,74	12,6	sandstone	x	brown	0,04
601,53	12,6	sandstone	x	brown	0,05
606,10	12,7	sandstone	a		
609,52	12,7	sandstone	a		
612,40	13,1	sandstone	r-?	brown	
617,60	13,1	sandstone	a		
619,93	13,1	sandstone	r-?	brown	
620,43	13,1	sandstone	r-?	dark brown	
625,14	13,1	sandstone	r-?	dark brown	
629,24	13,1	sandstone	a		
631,81	13,1	sandstone	a		
634,72	13,1	sandstone	r-?	brown	
638,23	13,1	sandstone	a		
638,30	13,1	sandstone	a		
642,08	13,1	sandstone	a		
644,03	13,1	sandstone	r-?	colourless	
647,77	13,1	sandstone	a		
654,80	13,1	sandstone	x	light-brown	0,05
655,30	13,1	sandstone	r-?	brown	
658,47	13,1	sandstone	a		
658,90	13,1	sandstone	r-?	brown, palagonitic	
666,03	13,1	sandstone	xx	brown	0,05
666,50	13,1	sandstone	x	brown, green	0,05
677,67	13,1	sandstone	a		
683,86	13,1	sandstone	a		
691,11	13,1	sandstone	x	brown, colourless	0,05
692,73	13,1	sandstone	a		
696,38	13,1	sandstone	x	light brown	0,05
701,12	13,1	sandstone	a		
702,48	13,1	sandstone	a		
704,83	13,1	sandstone	r-?	brown	
706,98	13,1	sandstone	x	brown	0,05
710,65	13,1	sandstone	x	brown, green	0,03
715,03	13,1	sandstone	a		
717,41	13,1	sandstone	r-?	brown, light brown	
720,97	13,1	sandstone	a		
725,46	13,1	sandstone	a		
731,28	13,1	sandstone	a		
733,67	13,1	sandstone	a		
735,32	13,1	sandstone	xx	brown, palagonitic	0,10
735,61	13,1	sandstone	xx	brown	0,05
737,05	13,1	sandstone	a		
743,03	13,1	sandstone	r-?	brown	
744,06	13,1	sandstone	a		
752,29	13,1	sandstone	r-?	brown	
752,44	13,1	sandstone	x	colourless, vesicular	0,05
756,00	13,1	sandstone	x	brown	0,10

(mainly quartz) in the silt and very fine sand-size range are scattered through the compacted organic matter.

At the time of this writing and on the basis of the lithological characterization of the sedimentary clasts from CRP-3, we can conclude that quartzarenite, siltstone and coal clasts are likely derived from various formations of the Beacon Supergroup that crop out in the Transantarctic Mountains, where all these described lithologies are well represented. The feldspathic arenites and wackes are presumed, on account of the dolerite fragments that they contain to have been eroded from older Cenozoic strata on the margin of the Victoria Land Basin.

X-RAY MINERALOGY

SEDIMENT BULK MINERALOGY

In order to generally characterize the bulk mineralogy of the sediments overlying “basement” in CRP-3, we analyzed 30 “fast-track” samples using a Rigaku Miniflex+ x-ray diffraction (XRD) system at the Crary Science and Engineering Center (CSEC). Two samples from the intrusion within “basement” also were analyzed, but those results are discussed separately below. The materials were analyzed, and the diffraction patterns were processed with JADE 3+ software, using procedures described in the CRP-1 *Initial Report* (Cape Roberts Science Team, 1998, p. 84-85).

Sample locations and the minerals identified in each sample are listed in table 4.4. Quartz is the dominant phase in each sediment sample, with feldspars (plagioclases and lesser amounts of K-feldspars) present in most samples. Illite is present in most samples above c. 143 mbsf, and a variety of clay minerals (including

mixed-layer clays and smectite) is present below c. 620 mbsf. Other minerals show low-intensity peaks on the XRD patterns, suggesting low abundances, and occur in only one or a few samples; these include augite, which is a detrital phase, pyrite, which is a diagenetic product, and analcime, which is identified with less confidence and may be a product of *in situ* alteration.

The data generated by these analyses cannot be used quantitatively to determine the abundances of the various minerals present. However, comparing the intensities of two XRD peaks (one chosen for each mineral of interest) can provide a useful qualitative indicator of variations in the relative abundances of those two phases through a stratigraphical section. The same peak area ratios have been calculated for CRP-3 samples as were used to determine total feldspar/quartz and K-feldspar/quartz ratios for the CRP-1 and CRP-2/2A *Initial Reports* (Cape Roberts Science Team, 1998, p. 84-85). The resulting stratigraphical profiles of feldspar/quartz and K-feldspar/quartz peak-intensity ratios are shown in figures 4.6 and 4.7, respectively.

The feldspar/quartz ratio profile (Fig. 4.6) shows relatively high values in the upper portion of the section (above c. 140 mbsf), generally low but variable values from c. 140 to c. 600 mbsf (with a single-point peak at c. 400 mbsf), and an increase to more consistent values below 600 mbsf. The K-feldspar/quartz ratio profile (Fig. 4.7) has a very different structure, with low values through most of CRP-3, and higher values only present at c. 257-408 mbsf and below c. 750 mbsf. One potential reason for these compositional variations is changes in sediment grain size, since feldspar/quartz ratios tend to decrease as grain size decreases (Blatt, 1992). Such a grain-size control does not appear to have been a major influence on these curves, however, because most “fast-

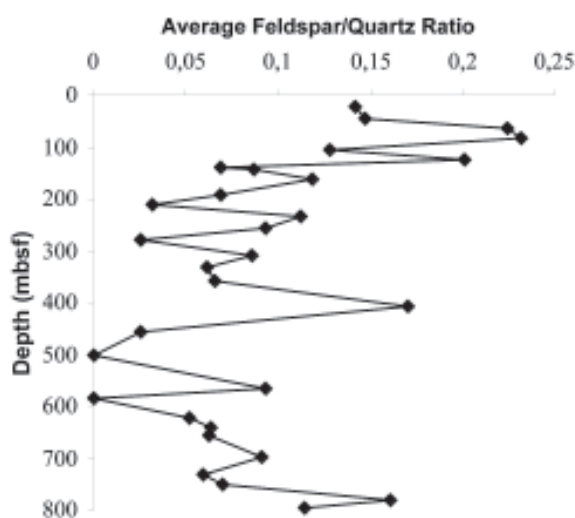


Fig. 4.6 - Stratigraphical profile of feldspar/quartz XRD peak intensity ratios for bulk sediments from CRP-3. Each ratio plotted is the average of three separate peak intensity ratios. The feldspar considered in these ratios is predominantly plagioclase.

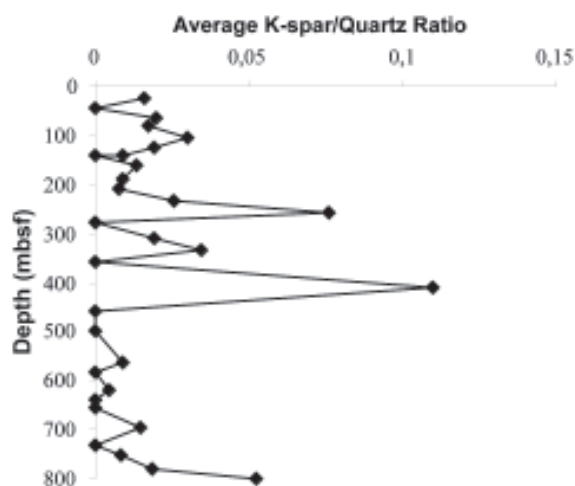


Fig. 4.7 - Stratigraphical profile of K-feldspar/quartz XRD peak intensity ratios for bulk samples from

Tab. 4.4 - Minerals identified by x-ray diffraction analysis in bulk samples from CRP-3.

Depth (mbsf)	Minerals Present
22.25	Quartz, plagioclase (albite and anorthite)
44.18	Quartz, plagioclase (albite and anorthite), K-feldspar (?sanidine)
63.00	Quartz, plagioclase (albite and anorthite), K-feldspar (orthoclase, sanidine, microcline), illite, ?augite
82.35	Quartz, plagioclase (albite and anorthite), K-feldspar (orthoclase), illite
106.40	Quartz, plagioclase (albite and anorthite), K-feldspar (orthoclase and sanidine), illite
123.65	Quartz, plagioclase (albite and anorthite), K-feldspar (orthoclase, sanidine, and microcline), illite
141.23	Quartz, plagioclase (anorthite), illite, minor pyrite, ?minor calcite
142.40	Quartz, plagioclase (albite)
162.14	Quartz, plagioclase (albite and anorthite)
190.79	Quartz
210.00	Quartz, plagioclase (anorthite), ?anorthoclase, ?mixed-layer chlorite/illite, analcime-C
232.47	Quartz, plagioclase (albite), K-feldspar (orthoclase and sanidine), illite
257.10	Quartz, plagioclase (albite), anorthoclase
278.53	Quartz, minor calcite
311.16	Quartz, ?plagioclase, mixed-layer clays (?chlorite/illite)
332.04	Quartz, anorthoclase, ?mixed-layer clays
359.29	Quartz, plagioclase (albite), ?mixed-layer clays
408.61	Quartz, plagioclase (albite and anorthite), K-feldspar (orthoclase and sanidine), chlorite to chlorite/illite mixed layer clays
457.40	Quartz, ?plagioclase
500.26	Quartz
564.43	Quartz, plagioclase (albite and anorthite)
584.47	Quartz
621.75	Quartz, mixed-layer clays (chlorite/illite or smectite/illite)
640.72	Quartz, mixed-layer clays (chlorite/illite or smectite/illite), minor plagioclase
656.54	Quartz, plagioclase (albite and anorthite), mixed-layer clays (chlorite/illite or smectite/illite)
697.40	Quartz, plagioclase (albite and anorthite), K-feldspar, mixed-layer clays (chlorite/illite or smectite/illite)
731.38	Quartz, plagioclase, mixed-layer clays (chlorite/illite or smectite/illite)
751.43	Quartz, plagioclase (albite and anorthite), mixed-layer clays (chlorite/illite or smectite/illite), ?K-feldspar
781.42	Quartz, plagioclase (albite and anorthite), K-feldspar (sanidine), smectite, illite/smectite mixed-layer clays
798.03	Quartz, plagioclase (albite and anorthite), illite, smectite, ?illite/smectite mixed-layer clays

track” samples were taken from zones with a significant sandstone component. As a result, the grain size of the bulk sediment analyzed does not appear to vary significantly between samples, thereby minimizing the possibility that the patterns observed in figures 4.6 and 4.7 are primarily a result of grain-size changes downcore.

A second possible explanation for the patterns seen in figures 4.6 and 4.7 is a change in sediment provenance during the period of deposition. The possible role of changes in sediment source can be evaluated by comparing the variations in bulk mineralogy, sand-fraction composition (see Sand Mineralogy section) and coarse-clast composition (see Basement Clasts section) downcore. This comparison indicates relatively consistent patterns of variation in all three compositional parameters, which aids in interpreting the bulk mineralogical data. Above *c.* 200 mbsf, the feldspar/

quartz ratio of the bulk sediment is relatively high, the feldspar/quartz ratio in the sand fraction is relatively high, and the clast population contains significant abundances of Ferrar Dolerite detritus relative to Granite Harbor Intrusives and sedimentary clasts. All of these lines of evidence suggest that Ferrar Dolerite exposures were a significant sediment source during deposition of the upper 200 m of CRP-3, and contributed feldspar-rich detritus that raised the feldspar/quartz ratio of the bulk sediment. The abundance of rounded quartz grains in the sand fraction has been interpreted to indicate that the lower Beacon Supergroup (the Taylor Group) was also a significant sediment source; the combination of abundant recycled quartz and little K-feldspar from the Ferrar Dolerite, therefore, produced the low K-feldspar/quartz ratios found in the bulk sediment above 200 mbsf.

From *c.* 200 to *c.* 600 mbsf, the feldspar/quartz ratio

The clay-mineral assemblage present above *c.* 410 mbsf suggests a predominance of physical weathering in the sediment-source regions, consistent with the evidence for glacially influenced deposition in the upper part of CRP-3. The shift to smectite-bearing assemblages below *c.* 650 mbsf may be explained in one of three ways: 1) that weathering conditions in the sediment source areas were wetter (and perhaps somewhat warmer) during deposition of the interval below *c.* 650 mbsf, 2) that the older sediment sources included volcanic rocks that were not present during deposition of the younger part of CRP-3, or 3) that diagenetic processes preferentially produced smectite in the deeper part of CRP-3. As discussed previously, the bulk-sediment mineralogy and the sand-fraction composition both suggest that Victoria Group rocks supplied detritus to the older section at CRP-3, based on increased abundances of feldspar and felsic-volcanic grains. Although cold-climate weathering of such grains might produce some smectite, it is also possible (and perhaps more likely) that the appearance of smectites records a shift to climates more favourable for chemical weathering. If the change in clay mineral assemblages does record a climatic shift, then this change may correlate with a similar compositional change that has been recognized in Southern Ocean cores and CIROS-1 (Ehrmann & Mackensen, 1992; Ehrmann et al., 1992; Ehrmann, 1997; Ehrmann, 1998a), and that lies just above the Eocene/Oligocene boundary (dated at 33.7 Ma on the timescale of Berggren et al., 1995). The palaeoclimatical and chronostratigraphical significance of this compositional change will be examined more closely in future studies. Finally, the appearance of these smectite-rich clays during microscope examination is reminiscent of the appearance of diagenetic clays found in other settings (see Calcareous Nannofossil section). This possible mechanism of formation will be evaluated by future studies of the clays using scanning electron microscopy.

BULK MINERALOGY OF THE INTRUSION AT 901.48-919.95 MBSF

Two samples from the intrusion within the "basement" at CRP-3 were analyzed for bulk mineralogy by XRD, using the same techniques as those employed to determine bulk-sediment composition. The samples analyzed are from 903.34 and 915.42 mbsf. The upper sample, taken from the altered and brecciated edge of the intrusion, contains quartz, feldspar (especially K-feldspar), illite, chlorite, mixed-layer clays (probably smectite/illite and illite/chlorite forms), siderite, and Mg-calcite. The lower sample, taken within the body of the intrusion, contains quartz, magnesite, smectite, mixed-layer clays (probably smectite/illite forms), kaolinite, Mg-calcite, and serpentine group minerals.

SAND GRAINS

The modal composition of the sand fraction in CRP-3 samples was examined to determine the range of sand-sized mineral and lithic grains present, to estimate their relative proportions, and to provide initial information on provenance and temporal variations. Previous studies in the area described sand grains and provenance of samples from the MSSTS-1 and CIROS-1 drill holes, both situated *c.* 80 km to the south, and in CRP-1 and CRP-2/2A, situated <1.5 km east of CRP-3 (Barrett et al., 1986; George, 1989; Smellie, 1998, in press). Like those authors, we report a varied provenance that resembles the local geology of the Transantarctic Mountains (TAM) in southern Victoria Land, including granitoid and metamorphic rocks of an Upper Precambrian-lower Palaeozoic 'basement', quartzose sedimentary rocks of the Devonian-Triassic Beacon Supergroup, and sills, dykes and lavas of the Jurassic Ferrar Supergroup (dolerite and basalt). A major difference with the previous studies, however, is a complete absence in CRP-3 of grains derived from alkaline volcanic rocks of the Cenozoic McMurdo Volcanic Group.

METHODS

For CRP-3, we selected *c.* 110 sandstone samples, which were impregnated with epoxy resin prior to making uncovered, unstained thin sections. Sampling intervals generally varied from *c.* 5-10 m, but only a few samples were suitable for counting at depths above 180 mbsf owing to substantial muddy matrices in those sandstones. We selected 71 samples for modal analysis for this report. One hundred grains were counted in each sample, exclusive of matrix (<30 µm), using the Gazzi-Dickinson point counting method. The modal data are summarised in table 4.6. Because of the low count total and lack of staining, the point counting results reported here should be regarded as qualitative. In particular, it was not practical to discriminate between plagioclase and alkali feldspar during counting and only total feldspar was recorded. However, because of the greater certainty of grain identifications compared to working with smear slides (*cf.* Cape Roberts Science Team, 1998, 1999), the CRP-3 modes are probably more reliable estimates of the sandstone modal compositions than those reported in previous *Initial Reports* of the project.

RESULTS

The CRP-3 sandstone samples range in grain size from very fine to medium/coarse but they are predominantly fine- to very fine-grained (*c.* 70% of samples). However, the proportion of these finer samples is lower than in previous CRP drill holes (*e.g.* 85% of counted samples in CRP-2/2A were fine- or very fine-grained; Cape Roberts Science Team, 1999). There is no

Tab. 4.6 - Qualitative detrital modes of sandstones in CRP-3, based on counts of 100 sand grains per sample and using unstained thin sections.

mbsf	Qr	Qa	Qtot	Ftot	P	Lv	Ls	Lm	Qp	Other
24,32	6	67	73	8	17	0	0	0	0	2
67,06	9	54	63	21	12	2	1	0	0	1
89,5	5	60	65	21	11	1	1	0	0	1
177,22	9	69	78	16	1	3	0	0	0	2
183,69	5	83	88	7	2	3	0	0	0	0
202,59	9	80	89	7	0	2	0	0	1	1
207,71	0	84	84	6	1	4	0	0	0	5
226,42	25	44	69	23	6	1	0	0	0	1
235,5	10	65	75	15	7	2	0	0	0	1
249,67	26	56	82	9	4	5	0	0	0	0
256,66	17	70	87	7	1	2	0	0	0	3
259,28	11	75	86	8	3	2	0	0	0	1
270,97	25	63	88	5	0	7	0	0	0	0
279,68	4	74	78	12	6	2	0	0	0	2
286,17	3	68	71	22	2	2	0	0	0	3
289,22	17	66	83	8	5	2	0	0	1	1
315,77	15	66	81	16	1	2	0	0	0	0
326,67	10	80	90	6	0	2	0	0	0	2
335,96	13	69	82	9	5	2	0	0	0	2
345,76	34	57	91	6	2	1	0	0	0	0
348,7	28	65	93	2	0	1	4	0	0	0
351,88	13	52	65	14	15	4	0	0	0	2
358,95	9	61	70	12	9	4	2	0	0	3
369,64	9	68	77	13	4	4	0	0	0	2
375,32	30	61	91	4	3	2	0	0	0	9
383,76	21	63	84	6	1	9	0	0	0	0
387,46	9	78	87	5	2	3	0	0	0	3
390,78	9	62	71	15	7	7	0	0	0	0
396,58	30	52	82	8	5	5	0	0	0	0
405,75	6	65	71	17	3	5	0	0	0	4
413,09	16	56	72	18	8	2	0	0	0	0
415,94	8	69	77	11	0	4	0	0	0	8
422,81	23	68	91	5	1	3	0	0	0	0
426,77	7	76	83	10	1	6	0	0	0	0
437,12	6	78	84	12	3	1	0	0	0	0
445,23	23	64	87	7	1	4	0	0	1	0
449,73	17	77	94	3	0	2	0	0	1	0
455,81	8	80	88	5	2	4	0	0	0	1
460,13	2	75	77	13	7	3	0	0	0	0
473,61	13	71	84	9	5	2	0	0	0	0
475,34	6	73	79	9	4	7	0	0	1	0
480,68	18	60	78	9	10	2	0	0	0	1
481,22	23	67	90	6	1	3	0	0	0	0
486,03	34	61	95	2	0	2	0	0	1	0
495,15	25	73	98	1	0	1	0	0	0	0
500,21	45	55	100	0	0	0	0	0	0	0
509,36	19	67	86	7	0	6	0	0	0	1
513,17	22	69	91	6	0	1	0	0	0	2
525,36	36	61	97	0	1	2	0	0	0	0
533,26	19	73	92	1	5	2	0	0	0	0
543,87	9	70	79	9	5	7	0	0	0	0
550,03	3	79	82	7	7	3	0	1	0	0
571,8	14	83	97	1	0	2	0	0	0	0
615,37	6	73	79	7	4	10	0	0	0	0
626,18	11	71	82	10	4	4	0	0	0	0
630,38	11	70	81	15	1	3	0	0	0	0
643,11	4	66	70	10	7	13	0	0	0	0
655,86	4	57	61	25	6	7	0	0	0	1
664,03	2	75	77	12	1	3	1	0	0	6
673,28	3	76	79	11	5	5	0	0	0	0
681,02	2	61	63	16	8	12	0	0	0	1
686,52	6	79	85	8	3	4	0	0	0	0
696,77	1	71	72	19	1	8	0	0	0	0
715,48	2	67	69	8	12	11	0	0	0	0
724,08	1	57	58	20	9	13	0	0	0	0
730,87	4	71	75	14	3	6	0	0	0	2
735,39	2	65	67	21	1	10	0	0	0	1
737,35	1	67	68	14	6	11	0	0	0	1
750,02	0	72	72	17	4	5	0	0	0	2
770,26	0	67	67	17	8	7	0	1	0	0
787,66	2	78	80	7	5	6	0	0	0	2

Abbreviations: mbsf - metres below sea floor; Qr - rounded quartz; Qa - angular quartz; Qtot - total quartz; Ftot - plagioclase and alkali feldspar;

P - pyroxene; Lv - volcanic lithic grains; Ls - sedimentary lithic grains; Lm - metamorphic tectonite grains;

Qp - polycrystalline quartz; other - accessory minerals (see text).

obvious systematic down-core variation in grain size, but samples coarser than fine sandstone are almost absent below 550 mbsf (only one sample). By comparison with previous studies (Smellie, 1998, in press), the most important effect of grain-size variations on the modal data set is likely to be increased data scatter, but the effect is unlikely to mask major provenance-related variations.

Mineral types encountered in CRP-3 are essentially identical to those described in previous CRP reports (see Cape Roberts Science Team, 1998, 1999). However, no alkaline pyroxenes or amphiboles, volcanic glass or fresh alkaline-volcanic lithic grains were encountered in CRP-3. The modal data are dominated by quartz (Q) and feldspar (F), which together usually comprise 86-97% of the mode (mean value *c.* 92%; Fig 4.8). Quartz occurs as rounded- to well-rounded (Qr) and angular- to sub-rounded grains (Qa), but the latter (Qa) are dominant and normally form >60% of the quartz-grain population (Fig. 4.8). Pyroxene (P) grains are also an important detrital component. The pyroxene is fresh and abundant in samples obtained above 180 mbsf, but it is invariably partially replaced by smectite (or rare carbonate) in lower samples. In the deepest samples, it is sometimes hard to distinguish smectite-altered pyroxene from abundant phyllosilicate cement, but fresh pyroxene relicts are usually present.

A variety of lithic grains is also present, forming up to 13% by volume. They include: dolerite; fine basalt; felsic lava; fine quartz-muscovite and ribbon-quartz tectonites; granitoids; polycrystalline quartz (Qp); graphic-textured grains; and a few grains of mudrock or rare muddy, very-fine sandstone (Ls). Several basalt types were distinguished, with variably lathy feldspar (corresponding to Group II volcanic clasts?; see section on Volcanic Clasts) or curved acicular to feathery feldspar or pyroxene crystallites (Group III volcanic clasts?; section on Volcanic Clasts), rod-shaped or rarely dendritic opaque oxide, and/or snowflake-textured devitrified groundmasses. The felsic lavas are formed of fine feldspathic or quartzo-feldspathic crystalline mosaics (chert-like) with scarce feldspar microphenocrysts. Granitoids are represented by grains of coarse polycrystalline quartz, and muscovite-quartz and quartz-alkali feldspar crystalline aggregates. Graphic-textured grains (*i.e.* composed of geometrically intergrown quartz and feldspar) are ubiquitous and may have had a source either in tholeiitic dolerite or granitoids. Fresh brown and very rare green and colourless glass grains were observed in smear slides, but were not encountered in any of the thin sections examined in the modal study (see section on Volcanic Clasts). All of the lithic-sedimentary (Ls) grains are conspicuously muscovite-bearing. A few may be syn-sedimentary, but Ls grains are generally very rare.

All other grain types are present in trace amounts (*i.e.* <<1% of the total mode). They include unaltered pale-green and pale-brown amphibole (hornblende), brown

biotite, muscovite, opaque grains (typically well rounded and probably mainly coal), zircon, sphene and garnet. Other, much less common accessories include bioclastic carbonate and silica, and epidote.

Most of the samples are cemented by a combination of phyllosilicate (rimming grains and as a pore filling) and/or carbonate, or else have a phyllosilicate-rich muddy matrix.

MODAL VARIATIONS

Quartz contents commence relatively low (60-75%) in samples below 180 mbsf but rise in samples below that depth (Fig. 4.8). A few samples are composed almost entirely of quartz, and most of the CRP-3 sandstones are more quartz-rich than any of the samples obtained in CRP-1 and CRP-2/2A. The proportion of quartz rises to a peak around 550 mbsf, and falls to lower values in the samples below that depth. Rounded-well rounded quartz grains are a conspicuous and characteristic feature of samples above 550 mbsf, but they rapidly diminish and become scarce below that depth. Feldspar contents vary antithetically to quartz, as also found in both CRP-1 and CRP-2/2A, but Q/F ratios show a slight gradual increase to 550 mbsf, falling at a steeper gradient thereafter.

Modal data for pyroxene are very variable, probably as a result of the low total counts for 100 grains (Cape Roberts Science Team, 1999). They generally form 2-10% of the mode, but pyroxene may be absent in a few samples. Conversely, pyroxene is more common (11-17%), and strikingly fresh, in samples above 180 mbsf, in part of the core dominated by dolerite clasts (see section on Distribution of Clasts). Other mineral grains (hornblende, opaque oxide, zircon, sphene, garnet) occur as 1-4 grains each *per* thin section. However, whereas opaque grains and zircon occur throughout the sequence, sphene and garnet are virtually absent below *c.* 475 mbsf (Tab. 4.7). Biotite occurs as free grains above 375 mbsf. Below that depth it is found only within quartz crystals.

No modal counts were made for the individual lithic-grain types, but petrographical observations indicate that dolerite and basaltic grains are ubiquitous (Tab. 4.8). They are particularly common above 180 mbsf, and there is a second zone with conspicuous dolerite grains between 480 and 530 mbsf. Granitoids and metamorphic tectonites are sparsely present down to 390 and 486 mbsf, respectively, and essentially vanish below. Finally, fine-grained felsic lavas also occur throughout the section. They are sparse above 280 mbsf but show a notable steady increase below *c.* 550 mbsf; they may be responsible for the observed increase in counts for total lithic grains to the base of the CRP-3 sequence.

PROVENANCE

All the grain types observed in CRP-3 have been described previously from cores recovered at other sites in the McMurdo Sound region, and they indicate a

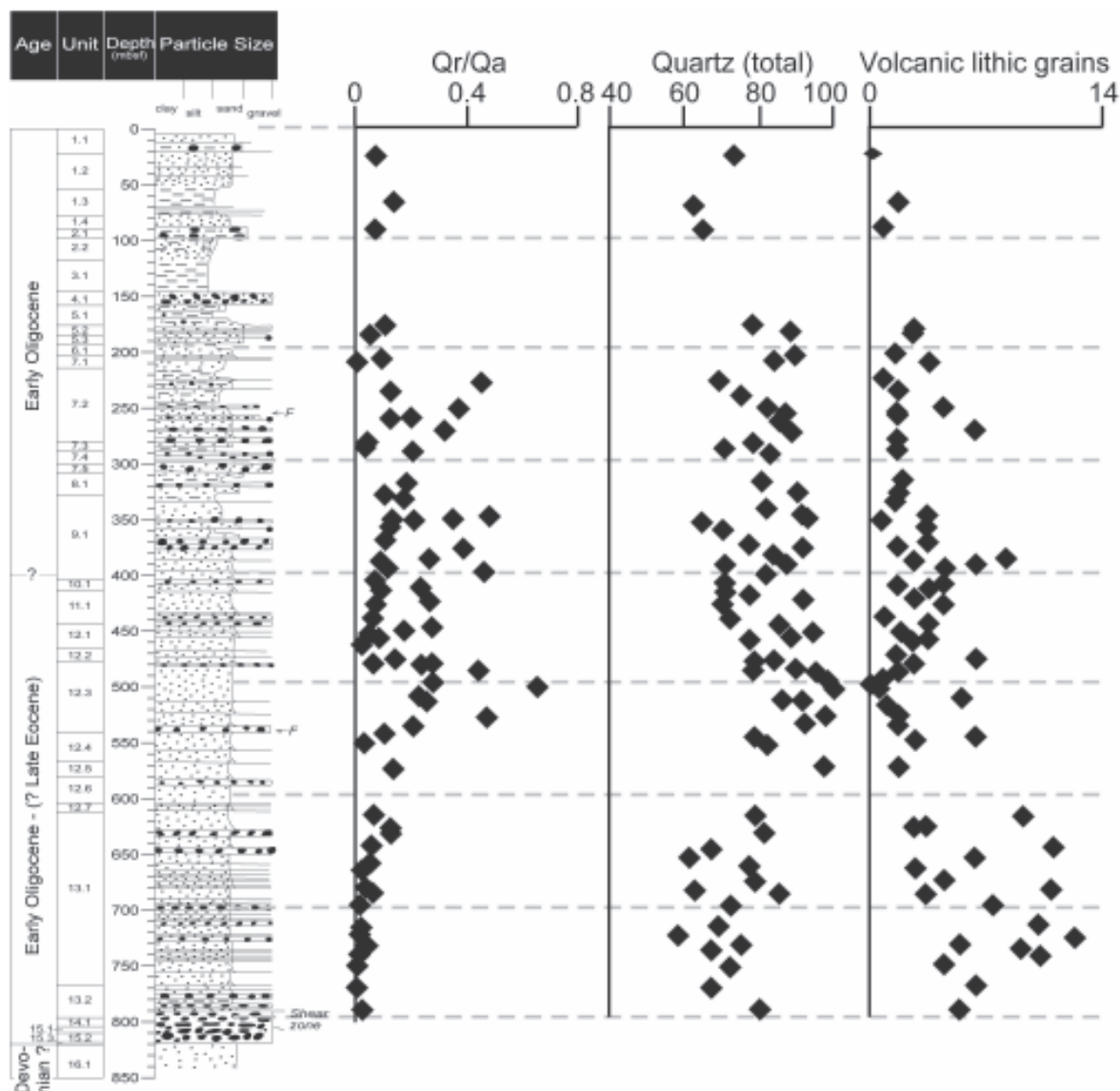


Fig. 4.8 - Summary diagram showing selected qualitative detrital modes for sand-grade samples from CRP-3, illustrating variations of compositional features with depth in the sequence. Note the several changes, present in all three modal parameters, which occur at *c.* 550 mbsf. Abbreviation: Qr/Qa – ratio of rounded to angular quartz grains.

similar, presumably local (TAM), provenance affecting all sediments. There is no evidence for a more distant source. However, whereas CRP-1 sandstones (mainly Miocene) were derived from a mixture of granitoid and volumetrically minor metamorphic ‘basement’ rocks (Beacon Supergroup sediments and Ferrar Supergroup dolerite), an important petrological transition was recorded in CRP-2/2A at 307 mbsf (upper Oligocene). That transition was interpreted by some to record an important downward change from granitoid- and Ferrar-dominated sediments above to mainly Beacon- and Ferrar-dominated sediments below, although both ‘types’ alternated in the lower half of the CRP-2/2A sequence

probably due to climatic influences (Smellie, in press; see also section on Tectonic History). The sandstones in CRP-3 apparently extend the trends observed in CRP-2/2A, with a clear continuing influence from Ferrar Supergroup detritus (dolerites and Kirkpatrick basalts). Ferrar-derived detritus is particularly important in the upper 180 mbsf. In addition, the high Qr/Qa ratios of most samples could indicate a provenance derived at least partly in the lower Beacon Supergroup (Taylor Group), in which rounded quartz grains are abundant (*cf.* Smellie, 1998, in press). By contrast, Qr/Qa ratios diminish progressively in samples below 550 mbsf. There are also significant changes in other modal values

Tab. 4.7 - Schematic summary showing the down-hole distribution of accessory minerals in CRP-3 sandstones.

mbsf	hornblende	biotite	muscovite	opaques	zircon	sphene	garnet	other
24,32	x	x?		x				
67,06		x		x		x		
89,5	x	x	x	x		x	x	epidote?, bioclastic carb
177,22	x	x		x				epidote
183,69	x			x	x			
202,59	x	x	x	x		x	x	
207,71	x		x	x	x		x	detrital carbonate?
226,42		x?	x (in qtz)	x				
235,5	x	x		x				
249,67								
256,66	x	x	x	x	x	x	x	bioclastic carbonate
259,28								
270,97								
279,68		x?	x	x				epidote
286,17	x		?	x	x	?		clinozoisite?
289,22	x			x	x	x	x	
315,77		x?	x	x	x			bioclastic carbonate
326,67	x	x	x	x	x	x		
335,96	x	x	?	x	x	x	x	
345,76	?		x (in qtz)	x	x			
348,7	x		x	x			x	
351,88				x				
358,95	x	x?		x	x		x	epidote
369,64	x			x				epidote
375,32		x (in qtz)		x	x		x	
383,76				x				
387,46	x			x	x	x	x	
390,78				x	x			
396,58	x							
405,75	x	x?	x	x	x		x	epidote
413,09					x			
415,94	x		x	x	x	x?	x	
422,81	x			x?	x		x	
426,77	x	x (in qtz)		x	x			
437,12	x			x	x	x	x	
445,23	x	x (in qtz)			x			
449,73	x		x	x		x?	x	
455,81	x	x	x		x	x	x	
460,13	x	x (in qtz)	x		x	x	x	
473,61	x			x		x		
475,34	x	x (in qtz)	x	x	x	x	x	epidote?
480,68	?				x			
481,22	x	x (in qtz)						
486,03	x		x (in qtz)					
495,15	x (in qtz)	x (in qtz)	x (in qtz)	x				
500,21		x (in qtz)			x			
509,36	x			x				
513,17	x			x				
525,36								
533,26	x	x (in qtz)	x (in qtz)	x	x (in qtz)			
543,87	x			x	x			
550,03	x	x (in qtz)		x	x			
571,8			x	x			x	
615,37	x			x		x		epidote
626,18	x	x (in qtz)	x	x	x			
630,38	x	x (in qtz)			x			
643,11	x	x (in qtz)		x	?			
655,86	x?		x	x	x			
681,02		x (in qtz)	x (in fsp)	x	x	x?		
730,87	x			x	x	x?		epidote?
737,35	x		x	x	x	x		
750,02	x	x	x	x	x	x		

Abbreviations: mbsf - metres below sea floor; qtz -quartz; fsp - feldspar

Tab. 4.8 - Schematic summary showing the down-hole distribution of lithic sand grains in CRP-3 sandstones.

mbsf	Lm	felsic Lv	Basaltic Lv (1)	Basaltic Lv (2)	dolerite	graphic	granite	Qp	Ls
24,32				x	X	x			
67,06			x		x	x		x	
89,5					x	x	x		
177,22		x?	X	x	X			x	x
183,69			X		x		x		
202,59	x	x	x		X	x			
207,71									x
226,42			X	x	x	x		x	
235,5	x				x	x		x	x
249,67									
256,66		x?			x				
259,28					x		x?		x
270,97									
279,68		x			x	x			
286,17		x				x			
289,22	x	x	x		x	x	x		
315,77		x	x		X		x	x	
326,67		x	x	x	x	x			
335,96	x		x						
345,76	x?	x		x	x		x	x	
348,7		x			x				x
351,88		x		x	x	x	x		
358,95	x	x			x				x
369,64		x			X	x	x		x
375,32				x	x	x		x	x
383,76		x	x	x	x	x	x	x	
387,46		x		x	x	x			
390,78		x			x			x	x
396,58			x		X		x	x	x
405,75	x	x		x	x			x	
413,09					x			x	
415,94	x?	x				x			
422,81		x			x	x		x	
426,77		X		x	x	x			
437,12	x	x							
445,23	x		X	X	x			x	x
449,73				x	x				
455,81		X				x			
460,13	x	x			x				
473,61	x	x			x			x	
475,34	x	x				x			
480,68		x		x	X	x		x	x
481,22		x		x	x	x			
486,03	x	x	X		X	x		x	
495,15		x		x	x			x	
500,21		x		x	x	x		x	
509,36		x		x					
513,17		x		x	X			x	
525,36									
533,26		x			X		x	x	
543,87		x	x		x	x		x	
550,03		X			x				
571,8		X			x	x		x	
615,37		x				x			
626,18		x	x		x	x			x
630,38	x?	X	x	x	x				
643,11		x	x	x	x	x			
655,86	x	X		x		x	x?		
681,02	x	X	x		x	x			
730,87		X	x	x		x			
737,35	x	X		x		x		x?	
750,02	x?	x		x					

x - present; **X** - dominant

Abbreviations: Lm - quartz-mica tectonite, ribbon quartz; Lv - volcanic lithic grains; Basaltic Lv (1) - fine basalts with feathery texture or rod-like opaque oxide; Basaltic Lv (2) - fine basalt with lathy plagioclase; graphic - graphic-textured quartz-feldspar; Qp - polycrystalline quartz, chalcedony; Ls - mudstone, sandstone (micaceous).

coincident with the change to lower Qr/Qa ratios: Q and Q/F ratios decrease, whereas F and volcanic lithic grains (Lv) increase (Fig. 4.8).

Some of the modal values of samples from below 550 mbsf in CRP-3 are similar to those in CRP-1 and CRP-2/2A sandstones derived from granitoids. Granitoids form a persistent 25% of the clast population right to the base of CRP-3, and a granitoid source is thus possible for the sand-grain population (see sections on Distribution of Clasts and Tectonic History). Conversely, the upper Beacon Supergroup (Victoria Group) is composed of sandstones that are more feldspathic, less quartzose, with few rounded quartz grains, and containing a significant proportion of felsic volcanic grains. It is also possible, therefore, that the CRP-3 sandstones below 550 mbsf were sourced in the Victoria Group. The trends observed and the virtual absence of rounded quartz grains could be interpreted to suggest that large outcrops of Taylor Group sandstones were not exposed in the period below *c.* 550 mbsf.

Finally, apart from rare grains of brown and colourless glass of uncertain composition (Kirkpatrick Basalt Group?), the absence of alkaline minerals, tephra layers and fresh volcanic lithic grains in CRP-3 strongly suggests that volcanism of the McMurdo Volcanic Group commenced at *c.* 25 Ma in the McMurdo Sound region (*cf.* Bellanca *et al.*, in press; Krissek & Kyle, in press; Smellie, in press) and did not extend back to Eocene times, as was formerly inferred (George, 1989).

IGNEOUS INTRUSION

PETROGRAPHY AND RELATIONSHIP WITH HOST ROCKS

LSU 17.1 comprises a magmatic body, intruded in the Beacon sandstones, that is deeply altered and brecciated at its margins.

We carried out detailed lithological observations on the core and sampling followed by a preliminary petrographical study of the thin sections and smear slides related to the intrusion and the host rocks. The data we obtained allowed us to recognize the following intervals:

a) interval between 900.40 and 901.09 mbsf, thickness 0.69 m: this interval includes the hardened portion of the Beacon sandstone (LSU 16.1) closely superjacent to the intrusion. In this interval the Beacon sandstone changes progressively downcore in colour, from pale red/brown (5YR6/6) to pale purple (5P2/2), and shows carbonate (Mg or Fe ?) or silica veins and incipient brecciation. However, there are no significant changes in the petrography and mineral assemblage of the rocks;

b) interval between 901.09 and 902.10 mbsf, thickness 1.01 m: breccia with angular and subangular fragments of the Beacon sandstones (maximum apparent size 15 cm) and the underlying intrusive rocks, immersed in a fine-grained brown (7.5YR4/4) matrix. Petrographically, the brown matrix appears to be composed of very abundant reddish hematite grains, smectite flakes, plagioclase microlites and very minor (and dubious) brown-glass shards. Igneous clasts (901.80 mbsf) are strongly weathered, although the rock texture is generally preserved: this is a hypocrySTALLINE, aphyric rock, with a few (<5%) large (2-mm) phenocrysts of which only the outlines are still recognizable. The clasts consist of tabular sericitised plagioclase and prismatic (augite ?) to equant (ortho ?) pyroxenes totally replaced by hematite, clay minerals and carbonate. The groundmass has a texture varying from intersertal to intergranular and is composed of altered subhedral plagioclases (now sericite). Between them, reddish hematite grains are abundant and probably have replaced mafic minerals. Interstitial areas with anhedral feldspars (albite or K-feldspar), smectites, serpentine and ilmenite needles are also found and have probably replaced original glass. The absence of quartz suggests that the glass was not more evolved than intermediate in composition. The largest sandstone fragment (901.30-901.45 mbsf) is angular, shows several carbonate-filled fractures and is bounded for most of its visible outline by a thin rim (0.5-1 cm) of chilled magma, pale green in colour. This indicates that it was formerly in close contact with the magma; it could be perhaps a portion of host rocks overhanging the intrusion or more probably a clast dislodged by the intruding magma. Petrographical analysis of the rim surrounding this country rock fragment was carried out through microscopic examination across the interface at 901.42 mbsf. The chilled margin here shows scattered mm-sized relic domains retaining a subophitic texture and partially altered plagioclase laths. These domains are set within a deeply altered brown groundmass (smectite?) that also includes lighter-coloured patches of chlorite ± serpentine (?), altered glass (?) and scattered grains of quartz (xenocrysts). Veins, 1 mm-thick and consisting of (Mg?) carbonate (±Fe hydroxide inclusions), intersect both matrix and relict domains. Carbonate also forms a continuous rim parallel to the contact between the intrusive rock and the sandstone. There is also a network of thin veins aligned parallel to the contact within the sandstone itself. The sandstone is a quartz-arenite consisting of rounded to subangular grains of quartz grains, polycrystalline quartz lithic fragments, K-feldspar and plagioclase, zircon and scattered deformed biotite. The contact zone consist of a 1- to 3-mm-thick layer

of carbonate-cemented sandstone with subrounded, coarser-grained quartz, minor K-feldspars (microcline) and zircon grains. No microscopic evidence of high-T contact metamorphism was detected. Very fine-grained greenish-phyllonite aggregates (sericite±chlorite intergrowth) occurring as interstitial phases, could represent a very low-T recrystallisation of an original clay matrix;

- c) interval between 902.10 and c. 918.00 mbsf, thickness 15.90 m: this zone includes most of the magmatic body. It is mainly massive and ranges in colour from blue-grey (5BG5/1), in the upper part, to purple (5P2/2), in the lower portions. On the whole, the rock forming the intrusion is highly altered even if some differences between different portions related to the depth seem to exist. The samples from the upper part (902.13, 903.30 mbsf) tend to preserve the original texture better although no original mineralogy can be detected. Petrographical features are similar to those of the clasts in zone b (see above), but the plagioclase in the groundmass tends to be more euhedral, hematite is less abundant, chlorite and smectite replacing mafic phases are more abundant than in the upper zone. In samples from the lower portion of the intrusion (912.22, 913.21, 915.00, 916.48 mbsf), the texture, as well as the original mineralogy, is totally destroyed: an anastomosing web of carbonates, smectites, probably serpentine, and hematite completely replaces most of the rock. The intrusion is crossed by several alteration veins or brecciated horizons filled by brown fine-grained material similar to that forming the zone b. A preliminary comparison (by means of smear slides) of matrix found in veins at different depths, suggested some variability: at 904.05 and 908.08 mbsf matrix is mainly chlorite and sericite, whereas at 905.20 mbsf smectite and sericite are the most abundant minerals and hematite and plagioclase grains are minor;
- d) interval between c. 918–918.95 mbsf, thickness 0.95 m: breccia with angular and subangular fragments, frequently deeply altered. Clasts belong both to the underlying Beacon sandstones and to the intrusion. They are immersed in a fine-grained brown (7.5YR4/4) matrix mineralogically similar to that observed in zone b;
- e) interval below 919 mbsf: the Beacon sandstone underlying the intrusion, shows a progressive change in colour, from purple (5P2/2) to light red/brown (5YR6/6), and a decrease of hardness with distance from the interface with the upper breccia.

CHEMISTRY

Four samples representing different horizons of the igneous intrusion (at 903.35, 909, 915.33, and 906.96 mbsf) were analysed for major and trace elements by XRF at Victoria University, Wellington. Results are reported in table 4.9.

The chemical compositions of these rocks confirm the occurrence of extensive weathering, as previously observed in thin sections. In all samples, major element concentrations appear to be strongly modified by alteration processes as large loss of ignition values (LOI) and normative corundum in the CIPW norm (Tab. 4.9) are detected. Thus, measured concentrations do not represent the original compositions of the igneous body and cannot be used to infer magmatic affinity.

However, significant differences exist among specimens: these are consistent with petrographical observations that indicate a primary effect of the weathering processes in the lower portion of the igneous body at a depth below 909.00 mbsf, although an original compositional zoning cannot be excluded. Specimens from the lower portion of the intrusion show highest LOI values, anomalously large iron contents and low silica concentrations. Highest iron content, associated with the largest LOI, can be mainly ascribed to the diffuse occurrence of Fe-carbonate (see also Clay Mineralogy section) and subordinately to the presence of haematite. In this case LOI would represent mainly the CO₂ loss.

Minor and trace elements show an analogous variability that can be ascribed to re-mobilisation due to alteration. However, some elements (Ti, P, Zr, Nb, Y) that are known to be less affected by alteration processes can still be used for comparisons with exposed igneous rocks and to infer the magmatic affinity. In figure 4.9 the samples of the CRP-3 intrusions are plotted in the classification-discrimination diagram of Floyd & Winchester (1978), based on ratios of immobile elements. Even though a significant scatter exists, they fall inside the subalkaline field, astride the divide between basaltic and andesitic compositions. These results rule out the parentage of these rocks with the alkaline Cenozoic magmatism and suggest rather a close correspondence with Jurassic Subalkaline rocks (Ferrar Supergroup). Also samples of the CRP-3 intrusion show Zr-Nb ratios quite close to those observed in Ferrar tholeiites (Fig. 4.10).

EMPLACEMENT STYLE AND HYPOTHESIS ON ORIGIN AND AGE

The geometrical relationships outlined above between the intrusion and the country rock and the petrographical characterization of the former can be used to make inferences on the emplacement and cooling styles of the intrusion. The inferred presence of glass in the magmatic rock points to relatively fast cooling of the margin of the magmatic body, whereas the occurrence of breccia in a clay-rich zone indicates an important episode of brittle deformation and hydrothermal alteration at a lower temperature that must have accompanied or followed the emplacement. The hydrothermal processes were sufficiently intense that the outer part of the intrusion (zone b and d) was mechanically and chemically modified. The lack of significant thermal metamorphic effects suggests that intrusion occurred in a short time

Tab. 4.9 - Chemical composition and CIPW norm of CRP-3 igneous intrusion.

sample	903.35 mbsf	906.94 mbsf	909 mbsf	915.33 mbsf
SiO ₂	56,53	54,00	34,24	38,52
TiO ₂	1,01	0,97	0,62	0,64
Al ₂ O ₃	24,57	20,97	15,91	15,29
Fe ₂ O ₃	4,87	8,55	20,64	18,46
MnO	0,01	0,06	0,16	0,18
MgO	0,92	1,23	2,19	2,74
CaO	0,57	0,80	2,40	3,78
Na ₂ O	0,56	0,63	0,19	0,12
K ₂ O	2,40	1,88	2,87	3,60
P ₂ O ₅	0,03	0,13	0,10	0,11
LOI	9,36	10,71	20,91	17,46
sum	100,83	99,93	100,23	100,90

CIPW Norm (Fe₂O₃/FeO=0.15)

Q	39,32	39,96	1,60	1,09
C	20,09	18,94	8,37	4,59
or	14,18	12,56	16,96	21,27
ab	4,74	6,03	1,61	1,02
an	2,63	3,53	11,25	18,03
hy	7,25	14,90	32,75	31,16
mt	0,84	1,67	3,56	3,18
il	1,92	2,08	1,18	1,22
ap	0,07	0,34	0,23	0,25

Trace Element (ppm)

As	1	12	2	0
Ba	179	198	577	521
Ce	38	65	29	30
Cr	75	73	150	135
Cu	77	90	110	93
Ga	22	19	21	21
La	15	18	21	10
Nb	7	8	5	4
Ni	36	57	51	98
Pb	9	16	9	8
Rb	70	75	64	181
Sc	47	73	52	53
Sr	84	150	61	56
Th	5	5	2	2
U	2	3	1	2
V	149	155	194	185
Y	13	27	34	50
Zn	42	66	584	131
Zr	163	144	95	98

Analysts :R. Grapes, J.E. Patterson
(Victoria Univ. Analytical Facility - Wellington, NZ)

span. The lack of vesiculation appears to exclude emplacement at shallow depths (*e.g.* neck or plug). The process responsible for the peripheral alteration could have been secondary boiling of the magma.

Even if chemical composition of the igneous intrusion points unequivocally to a parentage in Jurassic tholeiitic magmatism, its emplacement style shown in the CRP-3 intrusion is rather unusual for Ferrar dolerites. These normally show only a sharp contact with the host rocks (Roland & Worner, 1996). In addition, in Ferrar sills an extended crystallization due to a low-cooling rate

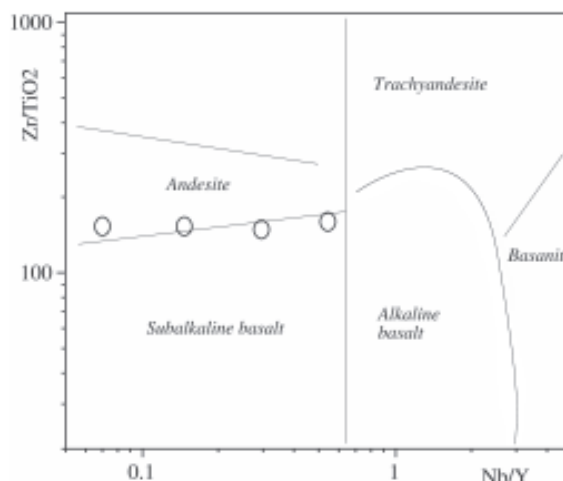


Fig. 4.9 - Discrimination and classification diagram according to Floyd & Winchester (1978). Open circles: CRP-3 igneous intrusion specimens.

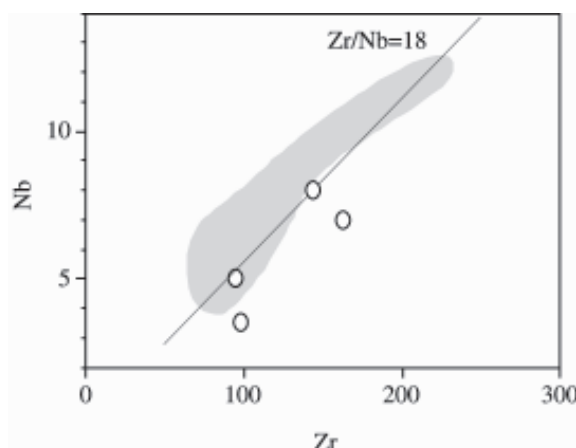


Fig. 4.10 - Correlation plot of Zr vs Nb. Open circles: CRP-3 igneous intrusion specimens; stippled area and best fitting curve are relative to Ferrar tholeiites of Hornig (1993).

produces very evolved residual liquids and quartz precipitation. These are lacking in the CRP-3 intrusion. However, fine-grained rocks with intergranular to intersertal textures were also found as clasts in CRP-3 (see Volcanic Clast section) and are known to form margins of some Ferrar sills (Elliot et al., 1995). On the other hand, some alkaline intrusions show important hydrothermal aureoles (*e.g.* Volcan Hills, Armienti et al., 1994) although chemical composition and mineral assemblages are very different from those of the CRP-3 intrusion.